NASA/TM-20205008006

# Development and Characterization of Lightweight Durable Composite Conductor for Cables

*Amjad Almansour, Dagny Sacksteder, Anthony Goretski, Jr., and Maricela Lizcano*
*Glenn Research Center, Cleveland, Ohio*

December 2021

# NASA STI Program . . . in Profile

Since its founding, NASA has been dedicated to the advancement of aeronautics and space science. The NASA Scientific and Technical Information (STI) Program plays a key part in helping NASA maintain this important role.

The NASA STI Program operates under the auspices of the Agency Chief Information Officer. It collects, organizes, provides for archiving, and disseminates NASA's STI. The NASA STI Program provides access to the NASA Technical Report Server—Registered (NTRS Reg) and NASA Technical Report Server—Public (NTRS) thus providing one of the largest collections of aeronautical and space science STI in the world. Results are published in both non-NASA channels and by NASA in the NASA STI Report Series, which includes the following report types:

- TECHNICAL PUBLICATION. Reports of completed research or a major significant phase of research that present the results of NASA programs and include extensive data or theoretical analysis. Includes compilations of significant scientific and technical data and information deemed to be of continuing reference value. NASA counter-part of peer-reviewed formal professional papers, but has less stringent limitations on manuscript length and extent of graphic presentations.

- TECHNICAL MEMORANDUM. Scientific and technical findings that are preliminary or of specialized interest, e.g., "quick-release" reports, working papers, and bibliographies that contain minimal annotation. Does not contain extensive analysis.

- CONTRACTOR REPORT. Scientific and technical findings by NASA-sponsored contractors and grantees.

- CONFERENCE PUBLICATION. Collected papers from scientific and technical conferences, symposia, seminars, or other meetings sponsored or co-sponsored by NASA.

- SPECIAL PUBLICATION. Scientific, technical, or historical information from NASA programs, projects, and missions, often concerned with subjects having substantial public interest.

- TECHNICAL TRANSLATION. English-language translations of foreign scientific and technical material pertinent to NASA's mission.

For more information about the NASA STI program, see the following:

- Access the NASA STI program home page at http://www.sti.nasa.gov

- E-mail your question to help@sti.nasa.gov

- Fax your question to the NASA STI Information Desk at 757-864-6500

- Telephone the NASA STI Information Desk at 757-864-9658

- Write to:
  NASA STI Program
  Mail Stop 148
  NASA Langley Research Center
  Hampton, VA 23681-2199

NASA/TM-20205008006

# Development and Characterization of Lightweight Durable Composite Conductor for Cables

*Amjad Almansour, Dagny Sacksteder, Anthony Goretski, Jr., and Maricela Lizcano*
*Glenn Research Center, Cleveland, Ohio*

National Aeronautics and
Space Administration

Glenn Research Center
Cleveland, Ohio 44135

December 2021

## Acknowledgments

The authors gratefully acknowledge NASA for funding this work as a part of its Transformational Tools and Technologies Project under the Aeronautics Research Mission Directorate. Also, the authors would like to thank Mr. John Setlock from the University of Toledo at NASA Glenn Research Center for his assistance with the electroplating processing. Additionally, the authors thank Mr. Alastair Gorven from Boise State University for his expertise in acoustic emission and frequency analysis. Finally, the authors thank Dr. Tiffany Williams from NASA Glenn for providing mechanical data on CNT yarns.

This work was sponsored by the
Transformative Aeronautics Concepts Program.



*Level of Review*: This material has been technically reviewed by technical management.

Available from

NASA STI Program
Mail Stop 148
NASA Langley Research Center
Hampton, VA 23681-2199

National Technical Information Service
5285 Port Royal Road
Springfield, VA 22161
703-605-6000

This report is available in electronic form at http://www.sti.nasa.gov/ and http://ntrs.nasa.gov/

# Development and Characterization of Lightweight Durable Composite Conductor for Cables

Amjad Almansour, Dagny Sacksteder,* Anthony Goretski, Jr.,* and Maricela Lizcano
National Aeronautics and Space Administration
Glenn Research Center
Cleveland, Ohio 44135

## Summary

Sustainable aviation in the form of electrified propulsion is likely to lead to an increase in the electrical components contained within a single aircraft. Moreover, the electrical resistance of copper (Cu) conductors is associated with power losses. As a result, it is desirable to design high-conductivity lightweight conductor materials, thus reducing the mass of components like motor windings, low-voltage signal cables, and transmission cables for data and power to improve the overall energy efficiency. One approach involves replacing pure Cu wiring with metalized carbon nanotube (CNT) composites. This report evaluates a framework for manufacturing composite conductor cables, measuring their electrical conductivity and strength, and modeling the overall conductivity and current sharing within such composites. Processing methods and parameters were refined. Tensile testing was conducted on the processed composite conductor cables with the use of acoustic emission and electrical resistivity to determine the strength and the failure mechanisms while monitoring the electrical conductivity. Cu-electroplated CNT samples from batch 5 outperformed pure Cu in conductivity and had comparable ultimate tensile strengths. The average of measured electrical conductivities of annealed Cu/CNT samples from batch 5 was greater than both theoretical predictions by 9.8 percent and was also greater than the conductivity of pure annealed Cu by 4.8 percent. Tensile strengths and conductivities are expected to improve with an additional densification step during processing. Theories explaining improved intrinsic conductivity are discussed, with a focus on chemical and mechanical interactions at the Cu/CNT interface. These include Cu infiltration of CNT crevices, CNT oxidation, activity at defects in CNT walls, and the release of carbide-forming metals from CNT walls. Validating any or all these theories will require further work replicating data, collecting and analyzing electron micrographs, and conducting chemical analyses.

*Summer Intern in Lewis' Educational and Research Collaborative Internship Project (LeRCIP).

# 1.0 Introduction

In the pursuit of sustainable aviation, there is great research interest in technologies for the power systems of turboelectric and 100-percent electric propulsion airplanes (Ref. 1). To achieve reductions in aircraft weight and power losses, it is beneficial that propulsion and power systems impose minimal load and use low electrical resistivity wires. One way to meet this demand is through the design of lighter and more electrically conductive cables. This report describes the research and development of lightweight Cu-metalized carbon nanotube (CNT) composite cables, which have the potential to surpass traditional Cu cables in specific electrical conductivity and mechanical strength. Cu/CNT composites have been identified as possessing the most promising balance of cost effectiveness and useful properties, with Al and Ag composites presenting secondary alternatives (Ref. 2).

Currently, wiring is often utilized in larger gauges; not for achieving higher electrical conductivity, but to accommodate the relatively weak mechanical strength of Cu (Ref. 3). A 2018 review of the state of the art of Cu/CNT composites describes the properties required of Cu/CNT composites if they are to be a viable candidate for replacing Cu wiring, such as mechanical durability, lightweightness, and electrical conductivity (Ref. 4). According to Sundaram et al., achieving a significant reduction in weight compared to Cu of the same gauge requires composites to contain at least 20 vol% CNT (Ref. 4). However, according to the models used in this study, this only affords an estimated 46 MS/m in conductivity. This is lower than the conductivity of pure Cu (59.8 MS/m) (Ref. 2). In general, wire resistance increases with decreasing cross-sectional area, as shown in Figure 1 (Ref. 5). Therefore, improving upon existing Cu cable requires the creation of cables that have a higher conductivity than Cu of the same gauge. CNTs possess high electrical conductivity and mechanical strength for their weight, making them good candidates for incorporation into lighter, higher performance composite materials.

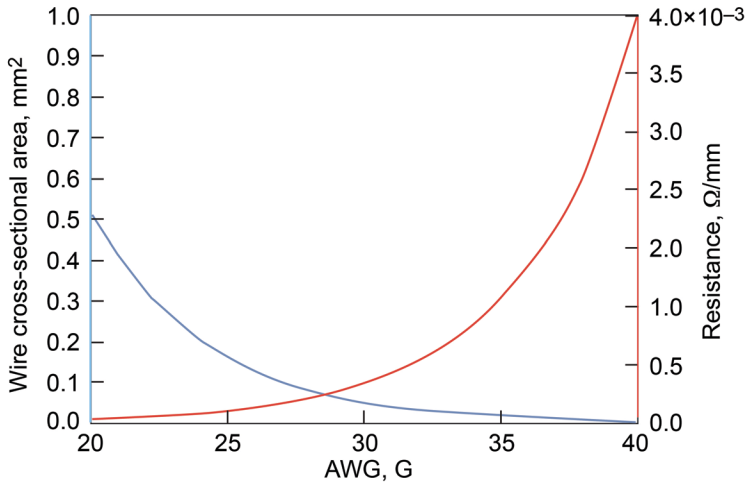


Figure 1.—Cross-sectional area and specific resistance versus Cu-based American Wire Gauge (AWG) (Ref. 5).

Various processing techniques yield composite geometries with significantly different electrical and mechanical properties. Powder processes necessitate a mixing step, which makes it impossible to control CNT alignment—a key aspect of the strength and conductivity of the wire. Another method of interest is electroless plating (Refs. 6 to 8). This method can improve the ultimate tensile strength beyond that of pure Cu (which ranges between 209 and 220 MPa) (Refs. 4 and 9). In one study, the electrical conductivity of samples made using this technique was maximized at 48.5 MS/m (Ref. 7). Wang et al. were able to produce composites with conductivity comparable to that of Cu (about 90 percent of the International Annealed Copper Standard, IACS) at 0.5 vol% CNT loading (Ref. 8). However, none of the samples in these studies surpassed Cu in electrical conductivity.

Compared to other application methods, electroplating has proven more promising for conductor cable uses (Ref. 4). With this setup, it is easier to select the CNT orientation and maintain high CNT percent volume. Cu/CNT yarn samples fabricated via electroplating also have demonstrated higher tensile strength (Ref. 10) and current-carrying capacity (Ref. 11) than pure Cu. A study of a composite made by electroplating Cu onto an aligned forest of CNTs resulted in a material with a lower coefficient of thermal expansion than Cu (Ref. 12). Electroplated composites proved to have better conductivity than their powder-processed counterparts, likely due to the better control of CNT alignment (Ref. 4). Nevertheless, Cu/CNT composites continue to fall short of theoretical predictions and targets for conductivity.

Shortcomings in electrical conductivity of the composite originate with the incorporation of CNTs into the otherwise very conductive Cu matrix. Not all CNTs possess the same electrical conductivity. CNTs can form with a variety of chiralities, shown in Figure 2. Chirality in CNTs is described by the two translational vectors $\mathbf{n}_1$ and $\mathbf{n}_2$ that connect the two halves of an atom in the tube wall that is split when the tube is “sliced and unrolled” into a theoretical sheet of graphene. When the sum $2(\mathbf{n}_1)+\mathbf{n}_2$ is a multiple of 3, the CNT is classified as metallic (m-CNTs) and possesses high electrical conductivity (Ref. 13).

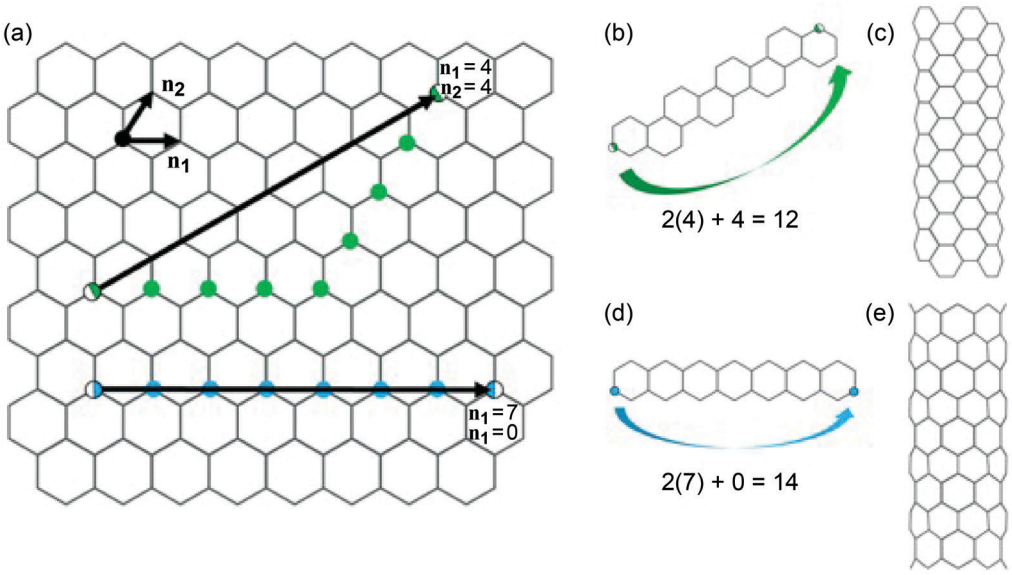


Figure 2.—Two example conformations of a carbon nanotube (CNT). (a) Two vectors $\mathbf{n}_1$ and $\mathbf{n}_2$ used to define relationship between two carbon atoms in theoretical sheet of graphene. (b) Graphene sheet is rolled such that it is to be connected at green atoms. (c) Resultant CNT has “armchair” conformation and is metallic. (d) Graphene sheet is rolled such that it is to be connected at blue atoms. (e) Resultant CNT has “zig-zag” conformation and is semiconducting.

CNTs of all other chiralities are considered semiconducting (s-CNTs). Any discrete estimate of the conductivity of CNTs is an average of the conductivities of s-CNT and m-CNTs. A random sample of CNTs consists of 33 percent m-CNTs, whose conductivity has been measured to be 50.7 MS/m (Ref. 2). The remaining nanotubes are s-CNTs, with lower conductivities. A calculation estimate suggests that the overall conductivity of CNTs is around 1.3 MS/m (Ref. 14). Thus, resistance within CNT yarn has two origins: intrinsic resistance within each nanotube and contact resistance between adjacent nanotubes (Ref. 13). Intertube contact resistance can be further classified as being (1) between two s-CNTs, (2) between two m-CNTs, or (3) between an s-CNT and an m-CNT. Because it is currently very costly to sort semiconducting and metallic CNTs, there is motivation to understand and mitigate the contact resistance interface between the two constituents. Contact resistance effects also extend to concerns about constituent interfaces within a composite—in this case, between CNTs and Cu.

Cu is understood to have poor affinity for CNTs because of its completely filled d orbitals in the ground state (Ref. 4). Increased electron density on the surface of CNTs renders it hydrophobic and likely also exacerbates electron-repulsive forces (Refs. 4, 15, and 16). Many approaches to improving the bonding of these two materials during electroplating have been proposed. The first method is functionalizing the CNT surface (Refs. 4 and 16). Oxygen-bearing functional groups on the CNT surface can potentially improve the initial adsorption of Cu onto the carbon surface through electrostatic interactions (Ref. 4). Although O atoms are electron-withdrawing, oxidation functionalization processes such as temperature treatment, acid reflux, and ozonolysis have been shown to improve the conductivity of uncoated CNTs (Ref. 17). Of these processes, dry ozonolysis initiated by ultraviolet (UV) radiation was found to generate the greatest increase in electrical conductivity (~1.7 MS/m) with the least amount of structural damage (Ref. 17). It has been proposed that reaction with an ozone molecule results in the CNT losing an electron, creating an electron hole in the CNT, which then functions as an additional charge carrier (Ref. 18).

In another approach to improving the Cu/CNT bond, Arai et al. added Janus Green B (JGB) to the electroplating bath, inducing a positive zeta potential on the CNTs and facilitating the codeposition alongside Cu ions (Ref. 19). This yielded samples with a conductivity around 50 MS/m. However, the geometry of codeposition tends to make it less suitable for cables, because CNT orientation cannot be controlled (Ref. 4). An alternative method involves the incorporation of carbide-forming metals into the metal matrix (Refs. 4, 20, and 21). In this case with a Cu matrix, a metal with incomplete d orbitals (such as Fe, Ni, Cr, Mo, Ti, Ru, or Al) is used (Refs. 4 and 20) to form a carbide on the metal surface and alloy with the Cu matrix to create a gradient bond layer (Refs. 2 and 22).

In addition to considering the intrinsic properties and bonding of constituents, it is important to understand and control the effects of microstructure on electrical conductivity and mechanical durability. Chawla et al. studied the relationship between porosity and composite conductivity by controlling the twist of uncoated carbon fibers (Ref. 23). With increasing twist, the mass of the composite became denser, increasing conductivity. The electrical conductivity was improved because of formation of junctions between adjacent fibers pressed together. Excessive twist led to diminished conductivity as well as the onset of fiber breakage. It is plausible that similar behavior would take place within similarly treated CNT yarns. Chowdhury found that an increase in the annealing temperature of codeposited Cu/CNT composites led to improved conductivity (Ref. 24). Annealing likely increased average grain size and eliminated vacancies, creating a more uniform lattice through which current carriers travel. Annealing also led to surface smoothing. This is noteworthy because surface roughness leads to more instances of electron scattering, increasing resistivity (Ref. 25). Shuai et al. were successful in creating film composites with Cu and super aligned CNTs whose tensile strength (287.2 MPa) surpassed that of pure Cu, with electrical conductivities up to 46.86 MS/m (Ref. 26).

Although the focus in the development of Cu/CNT yarns is the optimization of their electrical conductivity while maintaining mechanical strength, thermal properties are also of interest. The distinctive structure of CNTs lends them highly anisotropic thermal properties analogous to their electronic properties (the anisotropy factor for thermal conductivity in CNTs is 342) (Ref. 27). CNTs have good longitudinal thermal conductivity, making them well suited for heat transport. However, CNTs have extremely poor radial heat conductivity (Ref. 27). This anisotropy is a motivating factor for the use of Cu/CNT composites. CNTs can disperse the thermal load imposed on surrounding Cu conductor and insulation material, protecting against thermal runaway. Multiwalled CNTs (MWCNTs) were found to have slightly better heat conductivity than single-walled CNTs (SWCNTs), because their layered walls provided more possible phonon modes (Ref. 27). Bundling of CNTs resulted in a decrease in thermal conductivity, as adjacent nanotubes quenched the vibrational phonon modes of their neighbors. Cu/CNT composites have been fabricated with ampacities greater than that of Cu by up to a hundredfold, indicating improved temperature resistance of electrical properties (Refs. 26 and 28). However, electrical conductivities measured in these studies remain below that of pure Cu (46.86 MS/m (Ref. 26) and 47 MS/m (Ref. 28)).

In the present study, theoretical models were built to study the effects of metal coating types, critical metal thickness, composite porosity, and weight reduction on the composite wire's electrical conductivity. The metal coating's porosity was anticipated to have a greater effect on the total conductivity of the samples than the porosity of the CNT yarns. The two most promising composite systems (Ag-CNT and Cu/CNT) were selected for experimentation. Ag-CNT samples were fabricated using Ag paste, and Cu/CNT composites fabricated via physical vapor deposition (PVD) and electroplating. All samples were evaluated for surface quality and electrical conductivity. Four-probe electrical-resistance (ER) monitoring was used to measure the electrical conductivity of the processed composite wires. Batches of Cu/CNT electroplated composites were also tested for their mechanical durability. To track mechanical failure and changes in electrical conductivity, acoustic emission (AE) and ER monitoring techniques were used together. AE is appropriate for testing samples such as Cu/CNT composites with a high elastic modulus:density ratio. AE is also useful because it can be used to identify specific failure modes and locations (Refs. 29 and 30). A more efficient method for electroplating samples was designed. Parameters for plating, annealing, and surface preparation were refined. Results from the tensile tests with AE and ER monitoring provided new insights into the mechanical and electrical behavior of Cu/CNT composites in service.

Acronyms and symbols used within this report are listed in the appendix.

# 2.0 Experiment

The following subsections detail the fabrication of four sets of samples (painted Ag-CNT, PVD Cu/CNT, single electroplated Cu/CNT, and multiple electroplated Cu/CNT). In addition, procedures for conductivity and tensile strength measurements, as well as in situ AE and ER monitoring used during the tensile tests, are described. Finally, the approach and theory supporting modeling are outlined.

## 2.1 Processing

Painted Ag-CNT composites were fabricated by hand-brushing CI-1031-7 conductive Ag ink (Engineered Materials Systems, Inc.) onto either DexMat or Nanocomp Technologies, Inc., CNT yarn. In order to obtain meaningful conductivity measurements, coated samples were cured at 149 °C for burnout of organic paint binder. A Nanocomp CNT yarn was also coated via dipping to compare paint application

TABLE I.—MECHANICAL PROPERTIES OF MATERIALS USED TO MAKE Cu/CNT ELECTROPLATED COMPOSITES

| Constituent material | Elastic modulus, GPa | Tensile strength, MPa |
|---|---|---|
| Cu, cold worked (Ref. 9) | 112 | 344 |
| Cu, annealed (Ref. 9) | 125 | 209 |
| Nanocomp carbon nanotube (CNT) | 172±18 | 2,840±320 |

methods. DexMat CNT yarns were coated with Cu via PVD by Directed Vapor Technologies International (DVTI). For each PVD Cu coating thickness, there were three samples. Among these, one was tested as received, one was smoothed using a drawing plate, and the last was smoothed using a drawing block. Cu-electroplated samples were fabricated in house using Nanocomp CNT yarn. The CNT yarn was sent for analysis of strength properties. The mechanical properties of the Cu and CNT yarn constituents used in the electroplated composites are summarized in Table I.

Initial trials of electroplating of Cu on CNT yarns were conducted on a single CNT yarn. The initial electroplating setup consists of a Cu anode plate and single CNT yarn. The plate lengths, widths, and thicknesses were 152.4, 76.2, and 3.18 mm, respectively. The CNT yarn length was 154.2 mm. The anode plate and CNT yarn were placed inside a beaker filled with a $CuSO_4$-$H_2SO_4$ solution with deionized water. Current was drawn from a Hewlett Packard (now Keystone Technologies) 6633A constant-current power supply. A current setting of 0.1-A was applied for durations of 30, 60, and 90 min to coat CNT yarns individually with Cu coating thicknesses of 100, 200, and 300 μm, respectively. The initial electroplating trials were conducted to determine the feasibility of this processing method and compare the resulting conductivities of the fabricated composite wires with wires manufactured via different techniques. Next, a custom electroplating processing setup (shown in Figure 3) was designed to increase sample throughput and apply a more uniform Cu coating on the CNT yarn. It was created by three-dimensional printing a frame using acrylonitrile butadiene styrene (ABS), which was chosen for its structural integrity and low chemical reactivity. The setup involved an armature onto which one long strand of CNT yarn was wound, such that most of the length was vertical in the electroplating bath. The setup also involved two Cu anodes: one, a shroud surrounding the yarns and another, a rod placed between the yarns. This was to ensure a more even deposition onto the CNTs. For the electroplating setup shown in Figure 3, current was drawn from the same power supply equipment used in the initial setup. Additionally, the setup in Figure 3 was placed inside a beaker filled with a $CuSO_4$-$H_2SO_4$ solution with deionized water. Once the electroplating processing run ended, 152.4-mm Cu-coated CNT yarn samples were cut from that coated length and cleaned in ethanol. This electroplating setup enabled the electroplating of Cu on 52 CNT yarns for each processing run.

The CNT yarns were cleaned in ethanol prior to electroplating. If samples were removed from the electrolyte bath at any break in the electroplating process, they were again cleaned and ultrasonicated in ethanol to remove any contaminant that might impede even deposition of Cu. Samples were plated in a $CuSO_4$/$H_2SO_4$ solution with deionized water. The solution was first heated and saturated with $CuSO_4$. As the solution cooled, $CuSO_4$ precipitate fell out. The remaining solution was decanted and used for plating. Deposits of $CuSO_4$ appeared on the Cu metal electrodes and on the ABS rig. There was also a visible loss of material on the inner electrode. This suggests that the plated Cu was originating from both of the anodes and the cupric salt solution. Samples were plated for a total of 20 h. During the first 4 h, current was slowly increased to ensure a homogeneous deposition and prevent dendritic growth. Once a base layer had been established, a higher current was used to accelerate the process for the remainder of the plating time. Table II describes the experimental current settings that were used throughout the electroplating procedure.

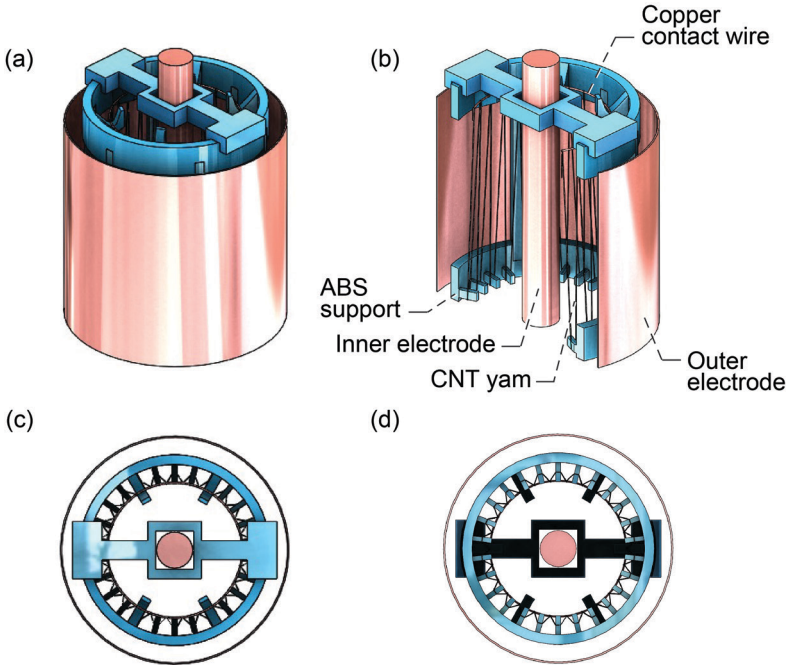


Figure 3.—Cu-carbon nanotube (CNT) electroplating setup, three-dimensional printed from acrylonitrile butadiene styrene (ABS). (a) Full view. (b) Cross-sectional view of setup strung with CNT yarn for plating. (c) Top view. (d) Bottom view.

TABLE II.—CURRENT SETTINGS FOR ELECTROPLATING FABRICATION OF Cu/CNT COMPOSITES

| Sample group (batch) | Current, A | | | | |
|---|---|---|---|---|---|
| | First hour | Second hour | Third hour | Fourth hour | Remaining 16 hours |
| 4 | 0.50 | 0.50 | 1.000 | 1.250 | 1.25 |
| 5 | 0.50 | 0.50 | 0.750 | 1.000 | 1.00 |
| 6 | 0.50 | 0.50 | 0.625 | 0.775 | 0.90 |
| 7, 8, 9, 11 | 0.35 | 0.50 | 0.650 | 0.800 | 0.95 |
| 10 | 0.30 | 0.45 | 0.600 | 0.750 | 0.90 |

Each plating group included 52 samples. Two samples from each plating group were annealed prior to tensile testing. Annealed samples were heated at 520 °C for 120 min. While in the furnace, samples were supported in a vertical position by a quartz tube. Samples from batches 4, 5, and 6 were annealed using Method 1, in which a quartz tube was first evacuated of air, then filled with Ar and sealed for the duration of heat treatment. Annealing Method 2 was used to heat treat samples from batches 7, 8, 9, 10, and 11. Method 2 annealing took place in an atmosphere of continuously flowing 4 percent $H_2$ (Ar balance). This change was made to prevent oxidation of the Cu from impurities in the pure Ar cylinder. It is also possible that these conditions enabled the reduction of any native oxide already existing on the Cu surface. Samples annealed in the presence of $H_2$ were visibly more lustrous.

## 2.2 Characterization

Micrographs providing characterization information about sample coating surfaces were obtained using a Phenom ProX G6 Desktop scanning electron microscope (SEM). Samples were conductive and thus were not mounted or coated for microscopy.

## 2.3 Testing

The strength of the materials was measured through tensile testing. These tests also included AE and ER monitoring to locate and characterize failures, and to correlate failure types to changes in conductivity. Figure 4 provides an illustration of the tensile testing with AE and ER monitoring setup.

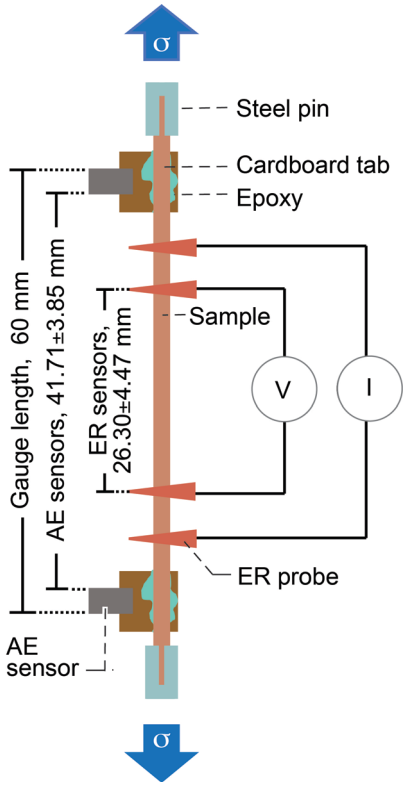


Figure 4.—Tensile test, indicating voltage (V) and current (I) measuring devices, acoustic emission (AE) and electrical resistance (ER) probes, and direction of applied stress, σ.

### 2.3.1 Tensile Testing

Monotonic fast fracture tensile loading was performed on the Cu electroplated composite wires using Instron frame model 5500R-4502 with a 500 N load cell and a displacement control loading rate of 0.127 mm/min. Both ends of the sample were inserted inside slotted steel pins. Duralco™ 133 epoxy resin (Cotronics Corp.) was injected into these slots to strongly bond the sample to the steel pins. Samples were then cured in a furnace at 83 °C for 4 hours. Next, Miller-Stephenson, Inc., two-part epoxy was used to affix 8- by 8-mm cardboard square tabs to the samples adjacent to the inner sides of the steel pins. AE sensors were later clamped to these cardboard squares. Afterwards, the steel pins were inserted into Instron tensile frame mechanical grips. The ultimate tensile stress (UTS) $\sigma_{c,UTS}$ of the composite wire was determined by dividing the maximum applied tensile load $F_{max}$ by the calculated composite wire's cross-sectional area $A_c$ (Eq. (1)). The $A_c$ of the wire was calculated using Equation (2) from averaged measurements of the sample diameter $d_c$, which was determined using calibrated calipers after plating. The CNT yarns diameter ($d_{CNT}$) was also computed from averaged measurements to be 100 μm using a caliper. CNT cross-sectional area ($A_{CNT}$) was assumed to be circular and calculated using Equation (2).

$$\sigma_{c,\mathrm{UTS}} = \frac{F_{\max}}{A_c} \tag{1}$$

$$A_c = \pi\left(\frac{d_c}{4}\right)^2 \tag{2}$$

All sample diameters are presented in Table III. The samples had an average diameter of 0.732±0.031 mm with an average cross-sectional area of 0.422±0.036 mm$^2$. The CNT volume fraction was calculated to be in the range of 1.7 to 2 percent using $A_{CNT}/A_c$. An average gauge length of 60 mm was used in all tensile tests.

TABLE III.—DIAMETERS OF COMPOSITES MEASURED WITH CALIPERS AFTER ELECTROPLATING

| Sample | Diameter, $d_c$, mm | Sample | Diameter, $d_c$, mm |
|---|---|---|---|
| 4U-1 | 0.760 | 4A-1 | 0.738 |
| 4U-2 | 0.710 | 4A-2 | 0.725 |
| 5U-1 | 0.777 | 5A-1 | 0.778 |
| 5U-2 | 0.757 | 5A-2 | 0.802 |
| 6U-1 | 0.758 | 6A-1 | 0.715 |
| 6U-2 | 0.735 | 6A-2 | 0.707 |
| 7U-1 | 0.730 | 7A-1 | 0.708 |
| 7U-2 | 0.708 | 7A-2 | 0.700 |
| 8U-1 | 0.735 | 8A-1 | 0.745 |
| 8U-2 | 0.725 | 8A-2 | 0.778 |
| 9U-1 | 0.765 | 9A-1 | 0.777 |
| 9U-2 | 0.703 | 9A-2 | 0.768 |
| 10U-1 | 0.705 | 10A-1 | 0.702 |
| 10U-2 | 0.688 | 10A-2 | 0.707 |
| 11U-1 | 0.705 | 11A-1 | 0.702 |
| 11U-2 | 0.697 | 11A-2 | 0.717 |

### 2.3.2 Electrical Resistance Monitoring

A calibrated Agilent multimeter (Model 34420A) with four probes was used to record electrical resistance (ER) with 0.15 percent accuracy. All electrical conductivity values for the composite were calculated from the ER measurements. These were conducted using the four-probe testing method described by Almansour (Ref. 29). Electrical leads were cleaned prior to testing with sandpaper. Equation (3) was used to calculate the resistivity ρ of the samples, where $R$ is the measured resistance, $L$ is the length between the two inner ER probes along the sample, and $A_c$ is the cross-sectional area of the composite wire sample. Electrical conductivity κ is taken as the reciprocal of the resistivity $\rho_c$:

$$\kappa = \frac{1}{\rho_c} = \frac{L}{A_c R} \tag{3}$$

Testing conditions varied slightly for different groups of samples. The Ag paint and Cu PVD samples were only tested without tension. The distance $L$ for these tests was 15 mm. The average diameter and cross-sectional area for the Ag paint samples were 0.659±0.491 mm and 0.509±0.609 mm$^2$, respectively. For the Cu PVD samples, the average diameter and cross-sectional area were 0.379±0.310 mm and 0.177±0.230 mm$^2$, respectively. The initial Cu-electroplated CNT samples used to evaluate the effect of surface smoothing were tested for conductivity without tension. The average ER probe spacing for these tests was 10 mm. The conductivity of the other Cu-electroplated samples that were processed using the setup in Figure 3 was measured during the monotonic tensile test without the application of tensile load. The baseline conductivity of these samples was taken to be the conductivity at time $t = 0$. The average distance between the ER probes at the beginning of these tests was 26.30±4.47 mm. The same diameter measurements of these samples that were used for tensile test calculations were used for conductivity calculations (see Table III).

### 2.3.3 Acoustic Emission Monitoring

Acoustic emission (AE) waveforms were recorded during specimen tensile loading using a Digital Wave Corporation four-channel fracture wave detector acquisition system and two B1025 piezoelectric AE transducers with 300 to 3000 kHz sensitivity. The AE sensors were spaced apart by 41.71±3.85 mm. The distance between the sensors was measured using a calibrated caliper. AE waveforms associated with events detected in the specimen gage section were filtered and analyzed using a software from Digital Wave Corporation. For each AE event, there is a waveform and wave energy recorded by each sensor. AE energy measurements from both sensors were averaged. In this experiment, the AE data analysis procedures of Maillet et al. and Gorven were adopted (Refs. 31 and 32, respectively), as their samples most closely represented the Cu/CNT composites. The frequency $f$ and frequency content $C(f)$ were used to calculate the frequency centroid $FC$ of the emission from each event of interest, using an original MATLAB® (The MathWorks, Inc.) script software (Eq. (4)). Signatures of specific failure mechanisms were identified in each tensile test. It should be noted that AE only collected meaningful information regarding the CNT; Cu is too ductile to produce strong acoustic signals as it fails. Failure of Cu was instead tracked by changes in electrical conductivity, determined via live ER measurements taken during the tensile test, as described above.

$$FC = \frac{\sum_{0^+}^{f_{\max}} C(f) * f}{\sum_{0^+}^{f_{\max}} C(f)} \tag{4}$$

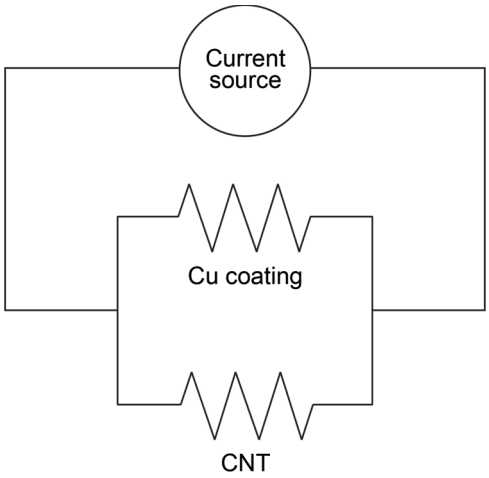

Figure 5.—Model circuit explaining nature of current sharing within Cu/CNT composite wire.

## 2.4 Modeling Methods

Theoretical modeling was used alongside experimental data to study the electrical properties of Cu/CNT composites as they relate to physical parameters. Models explored the effects of coating material, coating thickness, CNT porosity, and Cu porosity on composite conductivity and constituent current sharing. All conductivity models assumed that the Cu and CNT yarn behaved like two parallel resistors within the composite, according to the methods described by Almansour for unidirectional minicomposites (Ref. 29). A circuit schematic is provided in Figure 5.

To determine total conductivity in the composite, Equation (3) was used. The conductivities of composites made with either Cu, Al, or Ag metal coatings, applied at thicknesses between 25 and 800 μm were calculated. Equation (5) represents a modification of Equation (3), in which an allowance is made for porosity $X_y$ either in the metal (Cu) or in the CNT. Equations (6) and (7) were used to calculate the theoretical current sharing of the Cu and CNT constituents, respectively. In these equations, $I_y$% is the percent of current carried by the constituent and $V_y$ is volume percent of that constituent within the composite. Finally, all theoretical $t$ and experimental $e$ conductivity values were compared using Equation (8), a formula for percent change for generic properties $Z$. Equation (5) was also used to quantify weight reduction based on the rule of mixtures (ROM), where $\rho_y$ is the constituent resistivity.

$$\kappa = \frac{L}{A_c}\left[\frac{A_{\mathrm{Cu}}\left(1-X_{\mathrm{Cu}}\right)}{L\rho_{\mathrm{Cu}}}+\frac{A_{\mathrm{CNT}}\left(1-X_{\mathrm{CNT}}\right)}{L\rho_{\mathrm{CNT}}}\right] \tag{5}$$

$$I_{\mathrm{Cu}}\% = R\frac{A_c V_{\mathrm{Cu}}}{L\rho_{\mathrm{Cu}}} \tag{6}$$

$$I_{\mathrm{CNT}}\% = R\frac{A_c V_{\mathrm{CNT}}}{L\rho_{\mathrm{CNT}}} \tag{7}$$

$$Z = 100\left(\frac{Z_e - Z_t}{Z_t}\right) \tag{8}$$

## 3.0 Results and Discussion

The following subsections discuss modeling as well as results from processing and characterization of composite wires. Tensile test data are analyzed in conjunction with AE and ER monitoring information to provide insight on order and consequences of microstructural failures that take place over the lifetime of the sample. Conductivity results are presented and theories concerning the improvement in the intrinsic conductivity of the composite are addressed.

### 3.1 Modeling Results

Modeling was used to compare the behavior of three theoretical composites. Each composite was assumed to include a CNT yarn with a diameter of 100 μm. Resultant conductivities for Al, Cu, and Ag coatings of increasing thicknesses are shown in Figure 6(a). This information demonstrates that a significant improvement in conductivity can be achieved with a coating thickness of at least 200 μm and that coatings thicker than 300 μm offer minimal improvement in conductivity, as shown in Figure 6(b). Therefore, 300 μm was selected as the target coating thickness to maximize this benefit without oversizing the wire. In each case, the conductivities asymptomatically approached that of the pure metal as coating thicknesses increased (the conductivities of pure Al, Cu, and Ag at room temperature are 37.7, 59.8, and 62.9 MS/m, respectively) (Refs. 2 and 9). However, the conductivities of CNT samples hand coated with Ag ink were below conductivities predicted by the model. This was due to the process and form of Ag used. Remnants of organic binder from the ink were expected to still be in the coating. Additionally, Ag was not sintered to form a fully densified coating. Consequently, electroplating Ag was projected as the best approach to producing Ag/CNT composites. However, this was not attempted because Ag plating solutions are toxic and not environmentally friendly. Moreover, as de Groh assessed, the slight increase in conductivity provided by purer Ag would not translate into meaningful cost reductions for power transmission cable or motor winding applications (Ref. 2). Furthermore, Ag has a lower tensile strength than Cu, and would not have afforded any gain in mechanical properties (Ref. 9). Thus, Cu was confirmed as the best material selection.

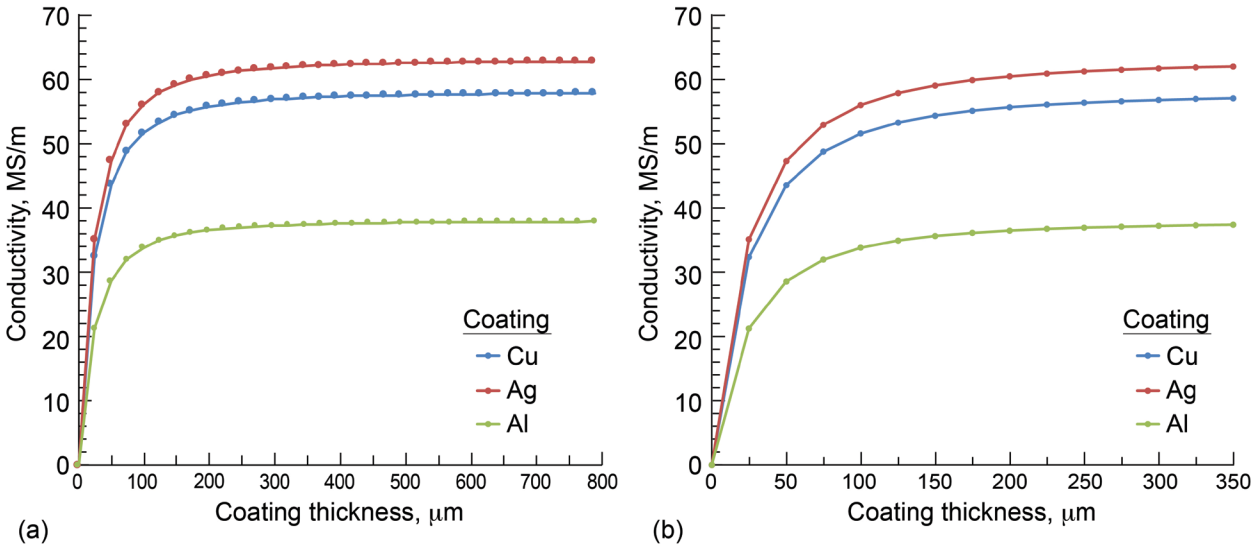


Figure 6.—Calculated theoretical electrical conductivity $\kappa_c$ of Cu/CNT, Ag/CNT, and Al/CNT composites with increasing metal coating thickness. (a) Conductivity to 800 μm thickness. (b) Closeup of conductivity to 350 μm thickness.

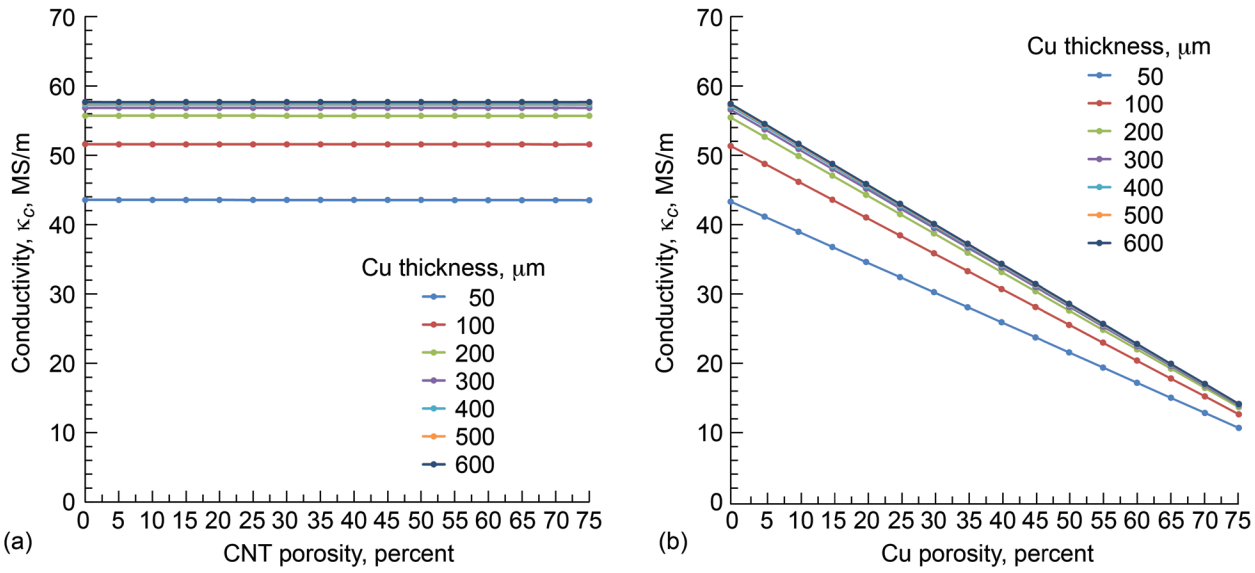


Figure 7.—Calculated theoretical electrical conductivity $\kappa_c$ of Cu/CNT composite (at CNT diameter $d_{CNT}$ = 100 μm and increasing Cu thickness) versus component porosity. (a) Changing CNT porosity $X_{CNT}$. (b) Changing Cu porosity $X_{Cu}$.

The models also were the basis for predictions about the mechanisms of electrical conduction in the sample. Altering the total porosity of the CNT (changing the volume percent of CNT) within the composite resulted in no significant change to conductivity of the composite (Figure 7(a)). This observation is supported by existing knowledge of electrical conduction in CNTs. Miao discusses how the intrinsic conductivity of CNTs relies predominantly on the splicing of CNT bundles, which leads to a well-integrated network of bundles within a yarn (Ref. 33). As a result, specific conductivity is not heavily dependent on porosity within CNT yarn in Cu-coated CNT yarn, where the absolute electrical conductivity of composite wire decreases slightly as CNT yarn porosity increases, since both the measured volume fraction and theoretical conductivity of the CNT yarn are lower than that of the Cu within the composite wire. Also, this decrease in conductivity can be attributed to a decrease in total cross-sectional area, not a fundamental change in the way charge carriers move through the material.

In contrast, increasing porosity in the Cu led to directly proportional drops in the electrical conductivity (Figure 7(b)). As shown in Figure 8, theoretical models predicted that Cu dominated the current carrying within the composite, even at high CNT content (i.e., low CNT porosity). This suggests that within the parallel resistor schematic framework (see Figure 5) larger differences in resistivity (and thus resistance) between the two constituents of the composite leads to the Cu carrying current away from the CNT yarn since electrical current in general prefers to take the least resistive path.

## 3.2 Influence of Processing Methods on Conductivity

Two methods for applying the Cu coating were compared: PVD and electroplating. The electroplated samples were fabricated using the initial setup for electroplating Cu on CNT. They were created to make a qualitative comparison of the feasibility and benefits of the two coating application techniques. As shown in Figure 9, the conductivities of electroplated samples were superior to that of the PVD samples for all Cu coating thicknesses. The difference between PVD and electroplated composite conductivity was due to poor bond quality in the PVD samples. Observations with an SEM revealed exposed areas of CNT on the PVD-coated samples. Furthermore, during manual smoothing, it was noted that the PVD samples

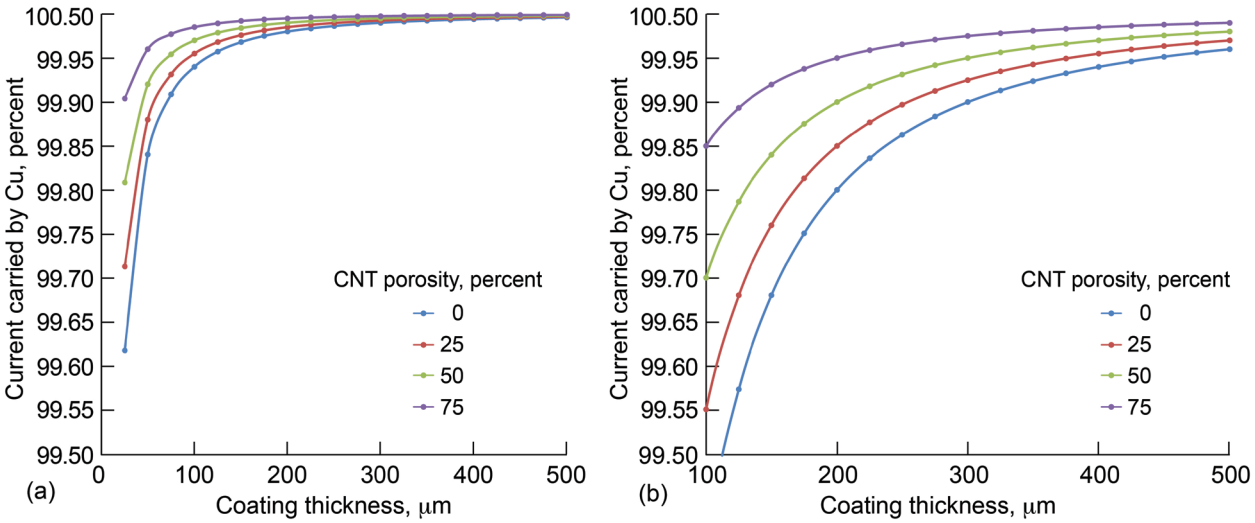


Figure 8.—Calculated theoretical percent of electrical current carried by Cu $I_{Cu}$% versus Cu coating thickness as function of increasing CNT porosity $X_{CNT}$. (a) Full percent range. (b) Close up of top of plot in (a).

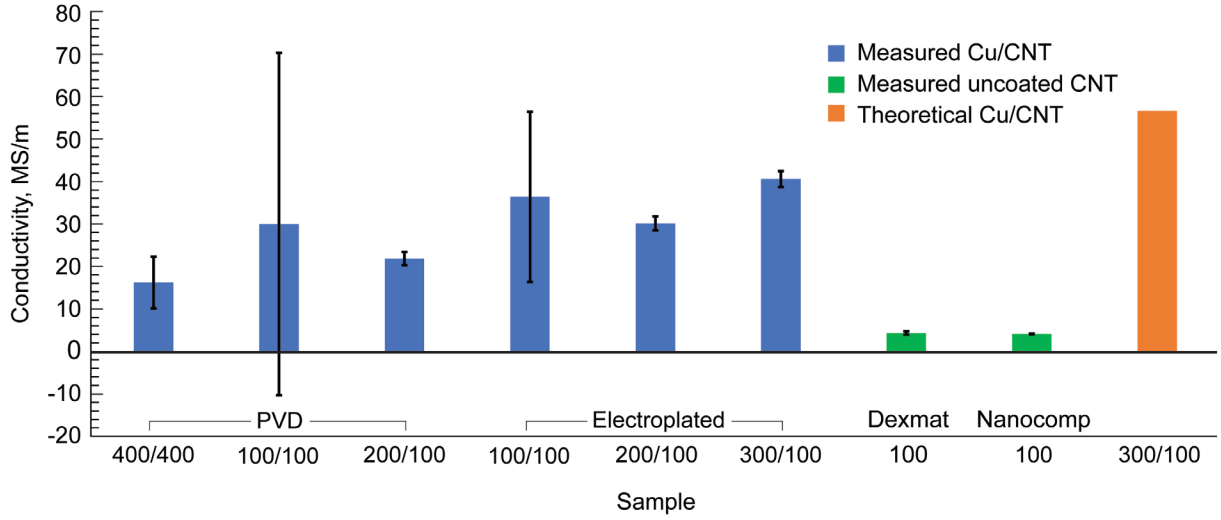


Figure 9.—Measured conductivities of Cu-PVD, Cu-electroplated, and uncoated CNT samples compared with modeled theoretical value. Coated sample geometries given as Cu coating thickness/CNT diameter in micrometers and uncoated, as CNT diameter. All dimensions are in micrometers. DexMat and Nanocomp Technologies, Inc., supplied CNTs in these experiments for PVD and electroplated samples, respectively.

were much easier to pass through the drawing block than the electroplated samples of the same diameter. Smoothing had damaged and removed sections of Cu coating on the PVD samples. It is believed that PVD is not suited for composites of this geometry, whose surface areas are small and nonplanar. All composite samples fell short of the theoretical prediction for conductivity in a 300-μm Cu/100-μm CNT composite. The effects of these phenomena can be seen in Figure 10, in which the as-fabricated PVD samples show some CNT exposure (Figure 10(d)) and the PVD-smoothed samples show large areas of removed or cracked Cu in Figure 10(b), (e), and (f).

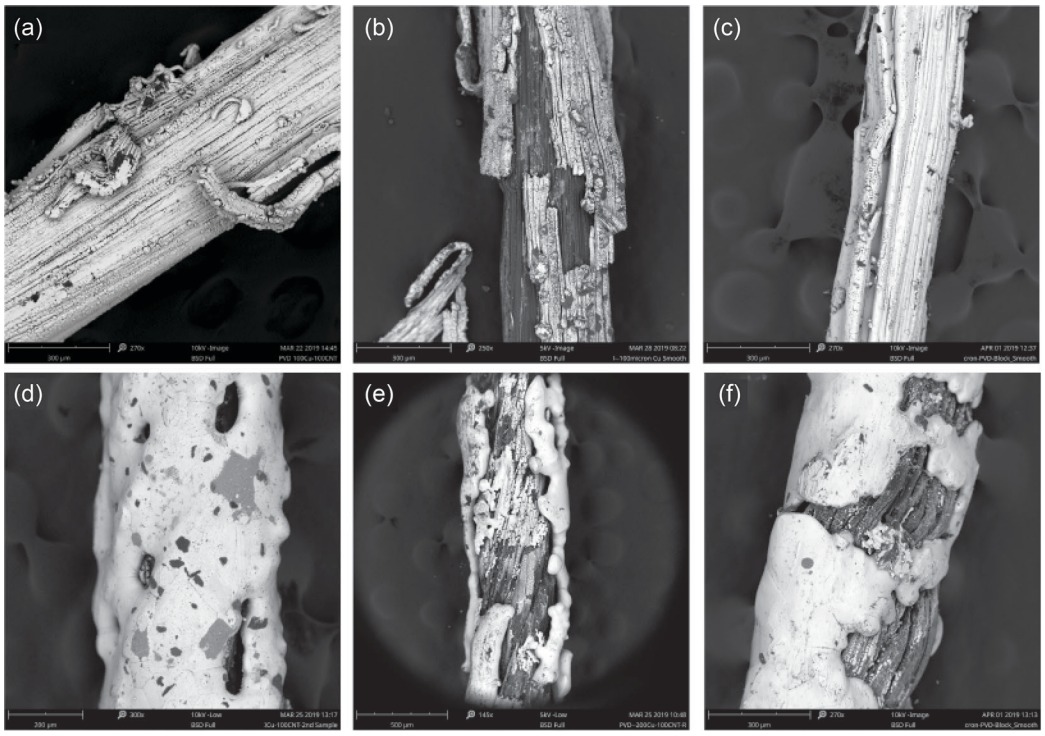


Figure 10.—SEM images of surface finish on PVD Cu/CNT composite samples. Dimensions are given as coating thickness/CNT diameter in micrometers. (a) Rough, 100/100. (b) Plate smoothed, 100/100. (c) Block smoothed, 100/100. (d) Rough, 200/100. (e) Plate smoothed, 200/100. (f) Block smoothed, 200/100.

## 3.3 Effect of Surface Roughness on Conductivity

Electroplated samples were difficult to smooth using manual tools. Samples became stuck in the drawing block, indicating a Cu/CNT adhesion resistant to debonding. Micrographs were used to compare surface coverage on rough and smoothed electroplated composites (Figure 11). No regions of exposed CNT were observed on either the rough or the block-smoothed samples.

Smoothing also appeared to have a positive effect on composite conductivity, as shown in Figure 12. This effect was more apparent in the samples with thicker coatings. However, the 100-μm Cu coating could not withstand the drawing-induced stresses, which led to cracking of the Cu coating. Meanwhile, samples with thicker Cu coatings (200- and 300-μm Cu-coated CNT samples) were able to sustain smoothing-induced stresses without total cracking. It is believed that the 300-μm Cu-coated CNT sample had the best conductivity because the increased metal volume could withstand the stresses of drawing and it provided a lower ER. This is supported by observations of cracking in the 100-μm Cu-coated CNT samples, presumably due to the formation of defects through the whole thickness of the coating. The difference in conductivities with respect to Cu coating thickness can also be examined at the atomic and subatomic particle scale: smoothing would have induced subsurface deformation in the Cu lattice, blocking the movement of charge carriers.

It is believed that smoothing samples at elevated temperature using a wire drawing machine would mitigate the effect of subsurface deformation on conductivity: Because most of these devices operate at elevated temperatures (Ref. 34), the defects formed by the force of the machine could diffuse and consolidate, relieving stress.

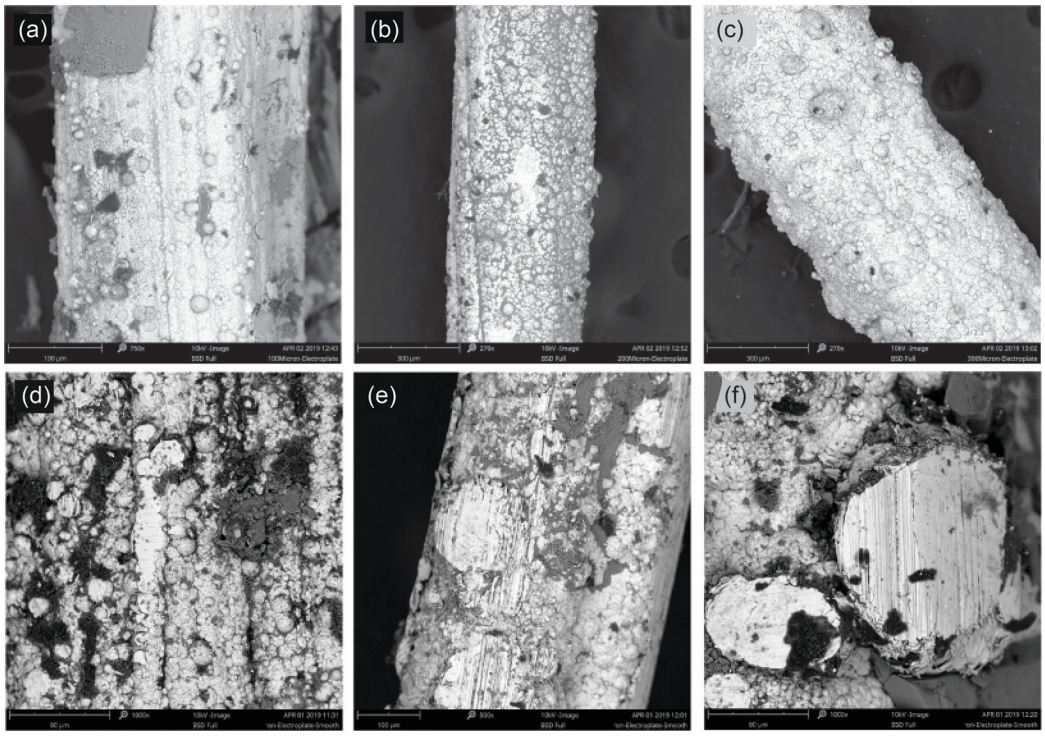


Figure 11.—SEM images of surface finish on electroplated Cu/CNT composite samples. Dimensions are given as coating thickness/CNT diameter in micrometers. (a) Rough, 100/100. (b) Rough, 200/100. (c) Rough, 300/100. (d) Block smoothed, 100/100. (e) Block smoothed, 200/100. (f) Block smoothed, 300/100.

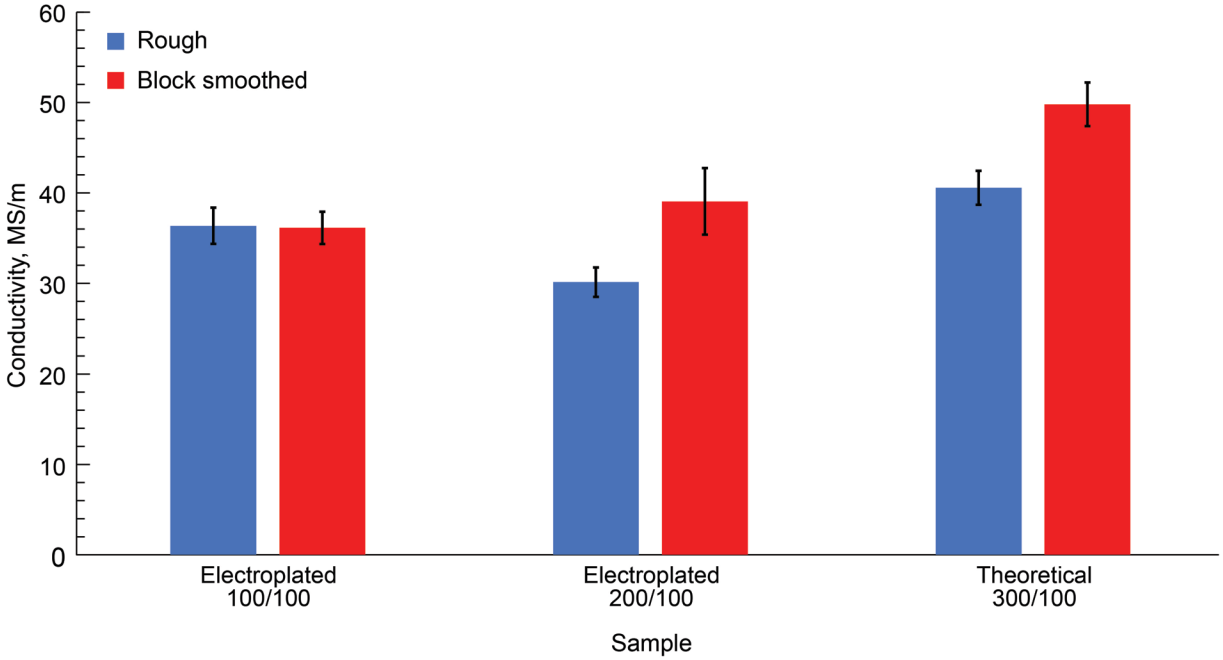


Figure 12.—Effect of surface finish on measured electrical conductivity of electroplated Cu/CNT samples. Dimensions are given as coating thickness/CNT diameter in micrometers.

### 3.4 Influence of Tensile Loading on Composite Wire Conductivity and Damage State

The ultimate tensile strengths (UTSs) of all samples are summarized in Table IV. The maximum load at the first peak in the stress-time curve was divided by the total cross-sectional area of the composite to yield an estimate of the composite UTS, $\sigma_{c,UTS}$. The UTSs of the unannealed and annealed electroplated samples from each batch were averaged and plotted (Figure 13(a)). The UTS results from the unannealed and annealed samples of batches 7, 8, 9, and 11 were also combined (Figure 13(b)) since they were fabricated with the same processing parameters. Because of a difference in sample size, this was done for qualitative appraisal of processing parameters, and the combined average cannot be used to make strict comparisons between batches. Overall, none of the samples from batches 7, 8, 9, or 11—unannealed or annealed—surpassed the tensile strength of Cu. Unannealed samples from batches 4 and 5 had tensile strengths similar (above and below) to that of Cu. The average maximum stress applied was 189.57±18.10 MPa for the unannealed samples and 156.90±40.51 MPa for the annealed samples. This trend is expected since annealing allows for grain growth and defect annihilation (Ref. 26). Equation (9) was used to compute the theoretical modulus of the composite wires, which is shown in Table IV. The elastic modulus $E = \sigma/\varepsilon$ (where $\varepsilon$ is strain) was used to relate the strength and modulus of the composite to the strength and modulus of the constituents. It was assumed that the strain of the composite was equal to both the strain in the CNT yarn and the Cu constituents at the onset of damage (first peak of the stress-time curve) since the conductivity did not drop significantly and there was no AE activity prior to the first peak, which indicates no significant damage in Cu or CNT had taken place in the composite wire yet. This isostrain condition, along with the ROM (Eq. (9)), was used to formulate Equations (10) and (11).

$$E_c = V_{\mathrm{CNT}} E_{\mathrm{CNT}} + V_{\mathrm{Cu}} E_{\mathrm{Cu}} \tag{9}$$

$$\sigma_{\mathrm{CNT}} = \frac{E_{\mathrm{CNT}}}{E_{\mathrm{C}}} \sigma_{\mathrm{C}} \tag{10}$$

$$\sigma_{\mathrm{Cu}} = \frac{E_{\mathrm{Cu}}}{E_{\mathrm{CNT}}} \sigma_{\mathrm{CNT}} \tag{11}$$

where $\sigma_{CNT}$ and $\sigma_{Cu}$ are the stresses partitioned in the CNT and Cu, respectively, at the time of the first peak in the stress-time curve. The composite stress at the first peak along with Equations (10) and (11) was used to partition the stresses on the CNT and Cu, as shown in Table IV. The strength of the composite wires in Table IV at the first peak is similar (slightly below or above) to the strength of the pure Cu reported in Table I. The stress on the partially loaded CNT at the onset of CNT damage in Table IV is an order of magnitude lower than the reported UTS of the CNT in Table I. This indicates that either the strength of CNT yarn was degraded through exposure to the $H_2SO_4$ plating solution, or the CNT yarn was fully loaded because of the undensified Cu being unable to carry a significant portion of the load due to the stiffness mismatch. In the case where CNT yarn was fully loaded at the first peak of the stress-time curve, the stress on the fully loaded CNT is expected to be $\sigma_c/V_{CNT}$, which is calculated in Table IV. However, the actual stress on the CNT should fall between the estimates of partial and full CNT loading. The samples that underwent tensile testing were not drawn because they could not be easily passed through the drawing block. It is believed that once a drawing machine setup has been configured for smoothing, these samples will demonstrate even greater strength. Compression of the Cu matrix during drawing will densify the material, improving mechanical strength. Additionally, densification is expected to improve conductivity within the Cu matrix as well as increase the quality of electrical contact between the Cu and CNT.

TABLE IV.—TENSILE PROPERTIES OF UNANNEALED AND ANNEALED Cu/CNT COMPOSITE SAMPLES

| Sample | Composite | | Copper | CNT | |
|---|---|---|---|---|---|
| | Elastic modulus, $E_c$, MPa | Tensile strength, $\sigma_c$, GPa | Tensile strength, $\sigma_{Cu}$, MPa | Tensile strength (partial load), $\sigma_{CNT}$, MPa | Tensile strength (full load), $\sigma_{CNT}$, GPa |
| (a) Unannealed. | | | | | |
| 4U-1 | 113.0 | 188.5 | 186.7 | 286.3 | 10.89 |
| 4U-2 | 113.2 | 220.5 | 218.2 | 334.5 | 11.12 |
| 5U-1 | 113.0 | 207.2 | 205.4 | 314.8 | 12.51 |
| 5U-2 | 113.0 | 233.6 | 231.5 | 354.8 | 13.39 |
| 6U-1 | 113.0 | 172.0 | 170.4 | 261.2 | 9.880 |
| 6U-2 | 113.1 | 166.6 | 165.0 | 253.0 | 9.002 |
| 7U-1 | 113.1 | 186.1 | 184.3 | 282.5 | 9.919 |
| 7U-2 | 113.2 | 183.6 | 181.7 | 278.6 | 9.206 |
| 8U-1 | 113.1 | 193.7 | 191.8 | 294.1 | 10.47 |
| 8U-2 | 113.1 | 198.9 | 196.9 | 301.8 | 10.45 |
| 9U-1 | 113.0 | 183.4 | 181.8 | 278.6 | 10.73 |
| 9U-2 | 113.2 | 110.5 | 109.3 | 167.6 | 5.462 |
| 10U-1 | 113.2 | 170.6 | 168.8 | 258.8 | 8.480 |
| 10U-2 | 113.3 | 176.7 | 174.8 | 267.9 | 8.365 |
| 11U-1 | 113.2 | 199.8 | 197.7 | 303.1 | 9.931 |
| 11U-2 | 113.2 | 189.0 | 186.9 | 286.5 | 9.180 |
| (b) Annealed. | | | | | |
| 4A-1 | 125.9 | 108.7 | 108.0 | 148.3 | 5.921 |
| 4A-2 | 125.9 | 101.5 | 100.8 | 138.4 | 5.335 |
| 5A-1 | 125.8 | 176.9 | 175.8 | 241.5 | 10.708 |
| 5A-2 | 125.7 | 162.5 | 161.6 | 221.9 | 10.453 |
| 6A-1 | 125.9 | 164.9 | 163.7 | 224.8 | 8.429 |
| 6A-2 | 125.9 | 170.9 | 169.7 | 233.0 | 8.543 |
| 7A-1 | 125.9 | 149.6 | 148.5 | 204.0 | 7.499 |
| 7A-2 | 126.0 | 147.3 | 146.2 | 200.8 | 7.219 |
| 8A-1 | 125.8 | 151.9 | 150.8 | 207.2 | 8.429 |
| 8A-2 | 125.8 | 112.3 | 111.6 | 153.3 | 6.799 |
| 9A-1 | 125.8 | 107.3 | 106.7 | 146.5 | 6.481 |
| 9A-2 | 125.8 | 64.3 | 63.9 | 87.8 | 3.794 |
| 10A-1 | 125.9 | 65.6 | 65.1 | 89.5 | 3.234 |
| 10A-2 | 125.9 | 172.7 | 171.4 | 235.5 | 8.633 |
| 11A-1 | 125.9 | 112.6 | 111.8 | 153.6 | 5.551 |
| 11A-2 | 125.9 | 88.9 | 88.3 | 121.2 | 4.571 |

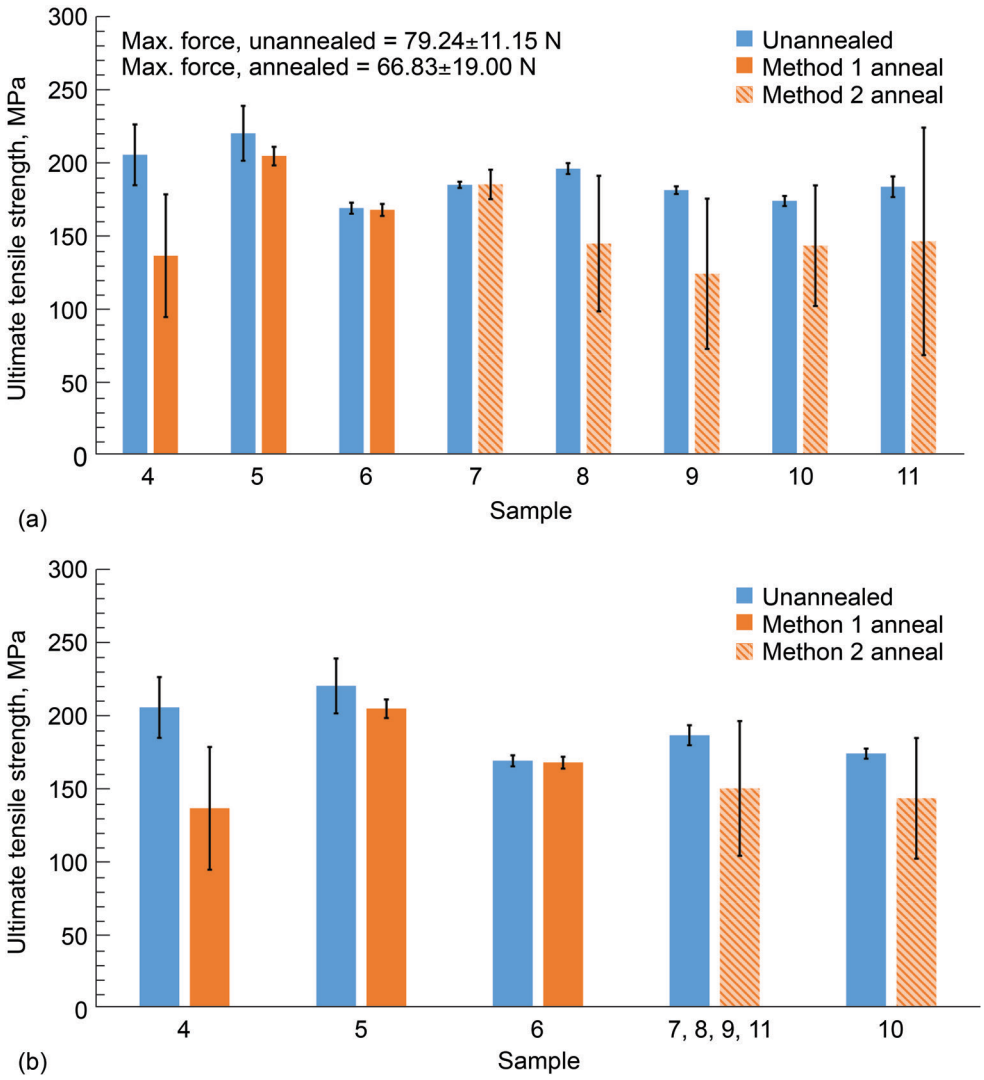


Figure 13.—Average ultimate tensile strength (UTS) of unannealed and annealed electroplated Cu/CNT composite samples. (a) Each plating batch. (b) Batches 7, 8, 9, and 11 combined.

A representative graph from the tensile test displaying the AE and ER data is presented in Figure 14. This plot reveals the chronology of mechanical and electrical failure. First, the stress on the composite wire increases as the Cu and CNT deform together elastically. The nonlinearity in the stress-time curve is attributed to some degree of delamination of Cu and CNT as the constituents debond from uneven load sharing between the Cu and CNT. The stress continues to increase, reaching the first peak in the stress curve, which signifies the onset of damage in the CNT. It is noted that many of the stress-time data sets contained smaller peaks on the shoulder of the first major peak; these smaller peaks represent additional damage formation and progression in the CNTs. After the CNT has begun to sustain damage in the first peak, the stress will increase on both the remaining intact portion of the CNT and the Cu. The gradual decrease in composite conductivity is caused by the ductile elastic behavior of the Cu. The stress on the Cu and the CNT continues to increase, which leads to a point where the Cu can no longer withstand the additional stress and begins to crack, causing a significant load drop. This is known to have originated from the Cu because there was no associated AE signal. The stress and conductivity of the composite drop as the Cu cracks propagate and lead to total failure of the Cu. In some experiments, a few remaining

strands of CNT yarn were observed to still be connected, and they could not support the sample mechanically or conduct a meaningful amount of current. It is important to note that the conductivity is relatively unaffected by the onset of damage in the CNT, thus establishing that composites can withstand mechanical damage and still function effectively as conductors. The slight continual drop in conductivity leading up to total failure can also be explained by Cu's Poisson response to tension, which causes a gradual reduction in effective cross-sectional area of the conductor. Additionally, piezoelectricity and piezoresistivity in both constituents may affect conductivity (Refs. 35 to 37). During electroplating, the CNT yarn, which is wound "hand-tight" onto the electroplating armature could be experiencing piezoelectric polarization (Ref. 37). It is possible that the plated Cu matrix would hold the CNT in tension even after plating, keeping the piezoresistive effect of the CNTs active within the composite. During the tensile test, the piezoresistive response of the CNT and Cu to applied tension would cause an active drop in conductivity. Overall, the stress-time curves obtained during tensile testing reveal an increase in toughness, marking improved durability.

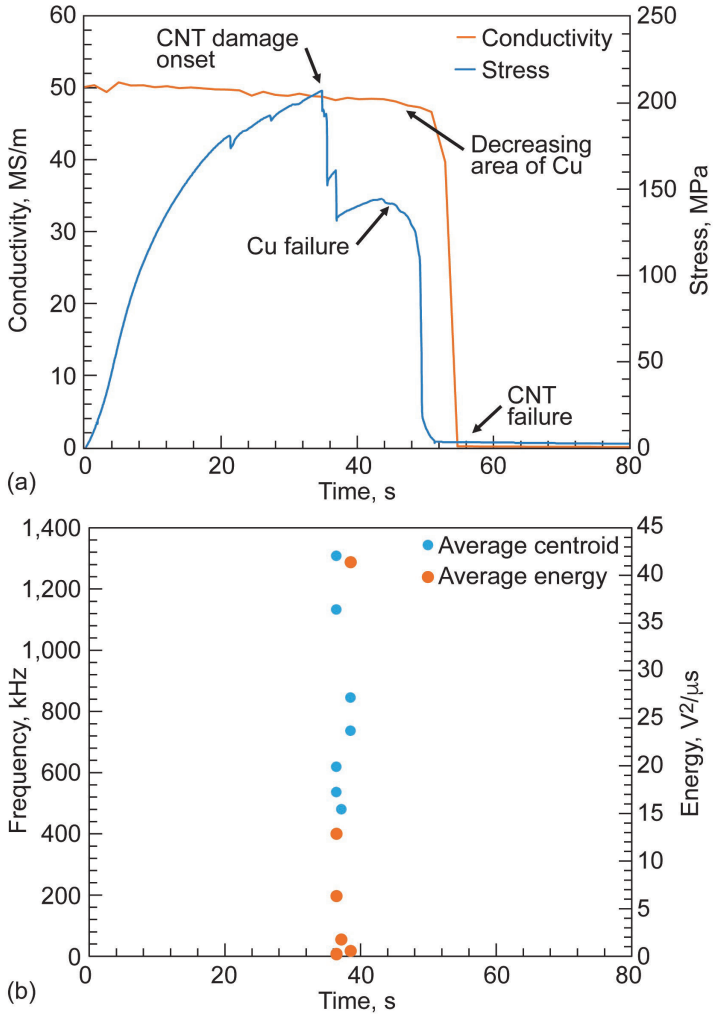


Figure 14.—Tensile test results for one unannealed Cu/CNT sample from batch 5. (a) Measured electrical conductivity and tensile stress evolution. (b) Acoustic emission events frequencies and energies.

## 3.5 Comparison of Conductivity in Electroplated Composites and AWG Cu Wires

Currently, Cu cables are used in sizes larger than is required for adequate conductivity to compensate for the relative mechanical weakness of Cu. Two of the samples in this study achieved conductivity higher than that of AWG Cu of the same diameter and cross-sectional area. A comparison of the studied samples and standard AWG Cu is presented in Figure 15. The average conductivity of the unannealed samples was 46.32±5.67 MS/m, and the average conductivity of the annealed samples was 47.45±7.61 MS/m. It is assumed that densifying these samples using a drawing machine setup would lead to an improvement in conductivity. The two annealed samples from batch 5 had conductivities greater than that of Cu (Figure 15(a) and (b)). The average conductivities of samples by electroplating batch are shown in Figure 16. It is assumed that the annealed samples had a larger average grain size, meaning there were less grain boundaries present to interrupt the flow of charge carriers.

The differences in conductivities between batches can be correlated by variations in the annealing atmosphere and plating conditions. Batches 4 and 6 were coated with the fastest plating procedures. Additionally, they were annealed in Ar according to Method 1. Because the Ar was not of absolute purity, it is likely that there was some air present in the annealing chamber during heat treatment. Samples from batches 4 and 6 were the only two groups for which the annealed samples averaged lower electrical conductivities than the unannealed samples. Annealing may have been detrimental to the conductivity of these samples because the Cu coatings may have become exposed to oxidizing contaminants in the Ar gas, which would have reacted with the Cu and promoted formation of the natural oxide layer. However, this does not explain why samples from batch 5 annealed using Method 1 outperformed unannealed samples from batch 5. This could be the result of batch 5 being plated under optimal conditions. The plating current “ramp-up” period decreased successively in batches 4, 5, and 6. Increasing current too quickly (batch 4) may have caused the initial layer of Cu to deposit too quickly, resulting in the formation of dendrites. In contrast, increasing current too slowly resulted in a coating that was too thin. This would match the variations in composite diameters listed in Table III. Overall, these results suggest that good bonding and Cu microstructure have a greater effect on conductivity than Cu coating surface changes that occur during annealing.

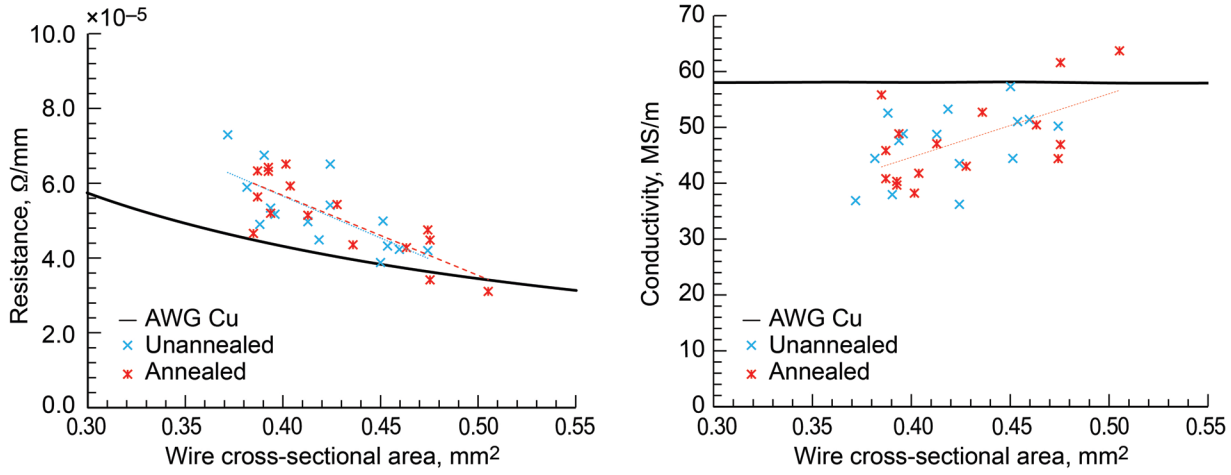


Figure 15.—Comparison of measured electrical properties of Cu/CNT composite samples and American Wire Gage (AWG) Cu. (a) Resistance. (b) Conductivity.

Batches 7, 8, 9, and 11 were coated using the same plating procedure and annealed according to Method 2 (a 4-percent $H_2$ in Ar circulating atmosphere). The conductivities across these batches are presented both separately and as one average in Figure 16(a) and (b), respectively (it is important to note that quantitative comparisons cannot be made in Figure 16(b) because of differences in sample size; the subplot is provided for qualitative perspective only). As a group, samples from batches 7, 8, 9, and 11 appear the most promising after batch 5. This correlates with the plating procedure, which was slightly slower than batch 5 but faster than batches 6 and 10. Batch 10 was also annealed using Method 2 but was plated using the slowest increase in current of all the samples. This resulted in a coating that was too thin, causing samples from batch 10 to have the lower conductivities. Annealing with Method 2 consistently led to an improvement in conductivity, suggesting that heat treatment in the presence of H reduces the native oxide on the Cu coating surface, improving purity in the main current-carrying constituent. The fact that all samples from batches 7, 8, 9, 10, and 11 had conductivities lower than the two samples of batch 5 supports the proposition that optimized plating parameters are essential in achieving optimal conductivity and good adhesion between the Cu and CNT.

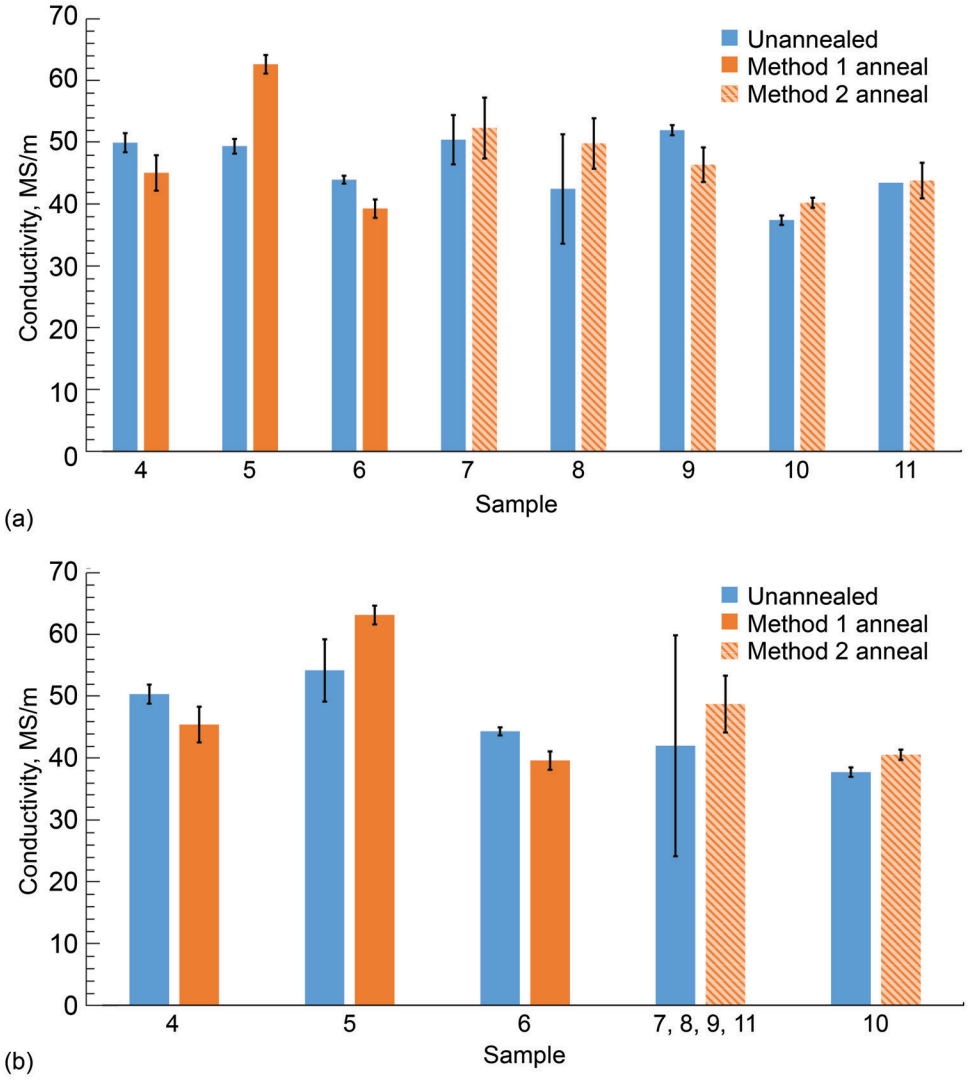


Figure 16.—Comparison of averages of measured electrical conductivities of unannealed and annealed electroplated samples by plating batch. (a) Each batch. (b) Batches 7, 8, 9, and 11 combined.

TABLE V.—PERCENT CHANGE IN EXPERIMENTAL CONDUCTIVITY OF Cu/CNT COMPOSITES (UNANNEALED AND ANNEALED) FROM THEORETICAL PREDICTIONS

| Sample group | Unannealed average change, percent | Annealed average change, percent |
|---|---|---|
| 4 | –12.3 | –20.8 |
| 5 | –5.7 | 9.8 |
| 6 | –22.8 | –30.9 |
| 7 | –11.3 | –7.9 |
| 8 | –25.4 | –12.6 |
| 9 | –8.7 | –16.8 |
| 10 | –34.1 | –29.2 |
| 11 | –23.5 | –22.9 |

The percent changes in conductivity between the theoretical and experimental composites are shown in Table V. The annealed samples from batch 5 outperformed the theoretical conductivities of these composites by 9.8 percent and the conductivity of pure annealed Cu reported by the International Annealed Copper Standard (IACS) by 4.8 percent, according to the parallel resistor model shown in Figure 5. Because conductivity is limited by intrinsic resistivity, the only way in which the annealed samples from group 5 could have surpassed both the predicted “parallel-resistor model” and pure annealed Cu conductivities is if there was a chemical change that led to a change in intrinsic electrical material properties. Given the materials and the processing parameters, it is unlikely that any new phase was formed. Instead, the nature of the Cu/CNT interface was modified. The following theories explore possible mechanisms for this modification, within the context of the correlated processing parameters discussed above.

The first consideration of the Cu/CNT interface is the degree to which the Cu ions were able to infiltrate the CNT yarn bundle. Previous studies of Pt-coated CNTs have revealed that during electroplating metal ions can enter defects in the nanotube (Ref. 38). The ions deposit solid metal and serve as seeds for subsequent plating. It is possible that a similar process took place in these Cu/CNT samples. If ions could penetrate atomic-level defects in the CNT wall, it follows that they would enter the crevices between the individual CNTs that make up a yarn. Overall this would yield a denser interface, creating good electrical contact between the two constituents of the composite. If plating occurred too quickly, Cu would deposit before infiltrating defects and crevices, leading to poorer coatings.

Secondly, oxygen-bearing groups on the CNT wall can potentially improve the adsorption of Cu on the nanotube surface (Ref. 4). However, there remains the concern that even if the Cu is able to access much of the total surface area of the CNTs, it is not well suited for chemically bonding with carbon. This is due to the ground state electron configuration of Cu, in which the *d* orbital is completely full. It is possible that the Cu is able to adhere to the CNT with the help of an intermediate alloy layer. As mentioned in the introduction, metals such as Fe, Ni, Cr, Mo, Ti, Ru, and Al have been used as bond coats in metal-CNT composites. Although no other metal was intentionally included during the plating process in these experiments, it is possible that trace amounts of transition metal catalysts like Fe, Co, and Ni were left behind after CNT fabrication, between the layers of the MWCNTs in the yarns (Refs. 16 and 39). Such metal atoms could potentially migrate towards the surface, forming a carbide layer to which Cu could more easily bond. It was previously found by Abel et al. that carbide-forming bond layers are only effective if applied evenly and with optimized thickness (Refs. 40 and 41). It is unlikely that any released catalytic metals would have been present in large enough quantities to act as a full bond coat. However, it is possible that in isolated instances, they facilitated the seeding of Cu at the defects from which they emerged, perhaps in conjunction with the Pt-CNT mechanism described above.

The probability of the release of trace amounts of metal catalysts is increased by the chemical conditions of the electroplating process. As described by Park et al., oxidation of CNTs via acid reflux leads to the formation of defects (Ref. 39). When defects occur in the wall of the CNT, they create openings through which the trapped trace metals can move, bringing them into contact with the Cu/CNT interface. Park et al. go further to suggest that the acids can then oxidize the escaped metals. However, in the context of electrochemical reduction occurring at the CNT surface, oxidation may not occur to this extent. Instead, the newly available metals may form a gradient bond layer, which on one edge forms a carbide with the CNT and on the other edge alloys with Cu. The initiation of CNT wall defects through acid reflux would also create more locations for Cu ions to form seeds for deposition.

Another mechanism by which trapped remnants of catalyst could be introduced into the system is through CNT unzipping. The mechanism for this reaction, catalyzed by Cu, is described by Wang et al. (Ref. 42). The unzipping reaction takes place in the presence of $H_2$ at temperatures between 200 and 300 °C. It is possible that such a reaction took place during annealing, which was done in a 4-percent $H_2$, Ar-balance atmosphere at 500 °C. Although the temperature is higher than what has been studied, this may have served to accelerate the diffusion of $H_2$ through the Cu to the Cu/CNT interface. Unzipped regions of CNT yarn would have released any encapsulated metals to take part in the carbide-forming reaction discussed above. This could have contributed to the overall improvement in constituent bonding and sample conductivity. Further investigation of H diffusion in this system and under these conditions is necessary to determine whether this mechanism is plausible. In addition, H could have entered the core from the cut ends, instead of diffusing through the Cu. Overall, the effects of annealing conditions and H dissolution on conductivity require further consideration for optimization.

The theory that acid from the electroplating solution led to the formation of defects in the CNT yarn is supported by observations in this study of frayed CNT yarn after exposure to $H_2SO_4$. In addition to creating seeding sites or enabling the release of helpful metal catalyst, acid reflux oxidation of the CNTs may have improved intrinsic conductivity by forming electron holes. As mentioned in the Introduction section, it was found that absorption of ozone during ozonolysis led to an electron transfer from the CNT to the ozone molecule (Ref. 18). It is known that exposure of CNTs to acid leads to the formation of epoxides and ethers in the CNT wall (Ref. 16). Although these functional groups are covalently bonded to the carbon structure rather than absorbed to the surface, the bonds could be polar enough to induce a permanent electron transfer from the CNT to the attached oxygen, essentially forming electron holes to act as charge carriers.

# 4.0 Conclusion

Modeling was performed to compare the effectiveness of different metal coatings in metal-CNT (carbon nanotube) composite wires for use as a lighter and stronger alternative to Cu conductors. It was found that Cu coating was the best compromise of conductivity, cost, and facile processing. Modeling also proved that increasing Cu porosity led directly to decreases in theoretical conductivity and established the optimal thickness for Cu (the main current carrier in such composites). Electroplating in acidic conditions was found to generate coatings with stronger interfacial bonds, more homogeneous coverage, and smoother surfaces than samples coated via physical vapor deposition (PVD). Experimentation with manual drawing tools corroborated that smoother surfaces lead to better conductivity, because of metal-matrix densification and reduced electron scattering. It was found that a Cu coating thickness of 200 μm is sufficient to avoid the formation of cracks in the Cu coating during the smoothing of the composite wire surface. The electroplating process parameters were optimized, and new samples were processed for combined conductivity and tensile testing of unannealed and annealed

samples. Tensile tests were conducted with acoustic emission (AE) and electrical resistance (ER) monitoring to detect the onset of damage in CNT within the composite wire and to monitor the wire electrical conductivity, respectively. Several samples demonstrated an ultimate tensile strength (UTS) similar to Cu. The UTS of each unannealed and annealed composite sample from batch 5 was greater than that of annealed Cu. It is likely that all processed samples will have even higher UTS if densified through wire drawing. Moreover, partial and full loading of the CNT yarns within the composite wires at the first peak of the stress-time curve were considered for analysis. Next, micromechanics was used to estimate the range of stresses on CNT yarns at the onset of CNT damage. Furthermore, live monitoring data established that Cu/CNT composites can continue to function as effective conductors even after they have been structurally compromised. The average measured electrical conductivities of annealed samples from batch 5 were greater than both theoretical predictions and pure annealed Cu by 9.8 and 4.8 percent, respectively. Theories for fundamental changes in structure and chemistry that would have led to an increased intrinsic conductivity include improved Cu infiltration of crevices and defects in the CNT yarn, CNT functionalization, the release and reaction of carbide-forming metals at the Cu/CNT interface, the formation of new seeding sites for Cu deposition, and fundamental improvements to CNT conductivity through electron-transfer chemistry. Further testing, electron microscopy, and chemical analysis of promising sample formulations will provide more insight into microstructure details and relevant conductivity mechanisms.

Finally, there are additional advantages of having the CNT yarn embedded in the center of the conducting wire via electroplating. The CNT yarn has the potential of removing heat away from the Cu/insulation interface. This would reduce the thermal aging of the insulation, increasing its performance life. Additionally, the Cu could also see diminished $I^2R$ resistive heating as heat is transferred from the Cu to the CNT yarn interfaces, resulting in enhanced electrical conductivity. Another advantage is that electroplating is a well-established manufacturing process that allows for an easy technology transfer and integration path for industry adoption with a much smaller investment cost compared to other CNT/Cu processing technologies.

# Appendix—Nomenclature

## Acronyms

| | |
|---|---|
| ABS | acrylonitrile butadiene styrene |
| AE | acoustic emission |
| AWG | American Wire Gauge |
| CNT | carbon nanotube |
| DVTI | Directed Vapor Technologies International |
| ER | electrical resistance |
| IACS | International Annealed Copper Standard |
| JGB | Janus Green B |
| MWCNT | multiwalled CNT |
| PVD | physical vapor deposition |
| ROM | rule of mixtures |
| SEM | scanning electron microscope |
| SWCNT | single-walled CNT |
| UTS | ultimate tensile strength |
| UV | ultraviolet |

## Symbols

| | |
|---|---|
| $A$ | cross-sectional area |
| $C(f)$ | frequency content of acoustic emission |
| $d$ | diameter |
| $E$ | elastic modulus |
| $F$ | force applied to sample |
| $f$ | frequency |
| $FC$ | frequency centroid of acoustic emission |
| $I$ | electrical current |
| $L$ | length |
| $\mathbf{n}_{1,2}$ | translational vectors connecting two halves of atom in CNT wall |
| $R$ | resistance |
| $t$ | time |
| $V$ | volume |
| $X$ | percent porosity |
| $Z$ | generic property |
| $\varepsilon$ | strain |
| $\kappa$ | electrical conductivity |
| $\rho$ | resistivity |
| $\sigma$ | tensile stress |

## Subscripts

| | |
|---|---|
| $c$ | composite (sample) |
| CNT | carbon nanotube |
| Cu | copper |
| $e$ | experimental |
| max | maximum |
| $t$ | theoretical |
| $y$ | composite constituent |

## References


1. National Aeronautics and Space Administration: Electrified Aircraft Propulsion (EAP). 2020. https://www1.grc.nasa.gov/aeronautics/eap/ Accessed June 22, 2020.
2. de Groh III, Henry C.: Consideration of Conductive Motor Winding Materials at Room and Elevated Temperatures. NASA/TM—2015-218882, 2015. https://ntrs.nasa.gov
3. Pops, Horace: The Metallurgy of Copper Wire. Innovations, Copper Development Association Inc., McLean, VA, 1997.
4. Sundaram, Rajyashree M., et al.: Copper/Carbon Nanotube Composites: Research Trends and Outlook. R. Soc. Open Sci., vol. 5, no. 11, 2018.
5. ASTM B258–18: Standard Nominal Diameters and Cross-Sectional Areas of AWG Sizes of Solid Round Wires Used as Electrical Conductors. ASTM International, West Conshohocken, PA, 2018.
6. Song, J.L., et al.: An Electroless Plating and Planetary Ball Milling Process for Mechanical Properties Enhancement of Bulk CNTs/Cu Composites. J. Alloys Compd., vol. 720, 2017, pp. 54–62.
7. Zhao, Shan, et al.: Cu Matrix Composites Reinforced With Aligned Carbon Nanotubes: Mechanical, Electrical, and Thermal Properties. Mater. Sci. Eng. A., vol. 675, 2016, pp. 82–91.
8. Wang, Hu, et al.: Novel Synthesizing and Characterization of Copper Matrix Composites Reinforced With Carbon Nanotubes. Mater. Sci. Eng. A., vol. 696, 2017, pp. 80–89.
9. ASM Handbook Committee: Properties of Pure Metals. ASM Handbook, vol. 2, ASM International, Materials Park, OH, 1990.
10. Randeniya, Lakshman K., et al.: Composite Yarns of Multiwalled Carbon Nanotubes With Metallic Electrical Conductivity. Small, vol. 6, no. 16, 2010, pp. 1806–1811.
11. Sundaram, R., et al.: Electrical Performance of Lightweight CNT-Cu Composite Wires Impacted by Surface and Internal Cu Spatial Distribution. Sci. Rep., vol. 7, no. 9267, 2017.
12. Subramaniam, Chandramouli., et al.: Correction: Carbon Nanotube-Copper Exhibiting Metal-Like Thermal Conductivity and Silicon-Like Thermal Expansion for Efficient Cooling of Electronics. Nanoscale, vol. 11, no. 4, 2014, p. 2089. https://pubmed.ncbi.nlm.nih.gov/30644937/ Accessed Dec. 20, 2021.
13. de Groh III, Henry C.: Highly Conductive Wire: Cu Carbon Nanotube Composite Ampacity and Metallic CNT Buckypaper Conductivity. NASA/TM—2017-219480, 2017. https://ntrs.nasa.gov
14. Almansour, Amjad; Lizcano, Maricela; and Goretski, Anthony: Lightweight and Durable Cable Design of Copper-Carbon Nanotube Composite Conductor Cables. Presented at the S&T Electrical Systems and Wiring Inter-Agency Meeting, Cleveland, OH, 2019.
15. Arysomayajula, Lavanya; and Wolter, Klaus-Juergen: Carbon Nanotube Composites for Electronic Packaging Applications: A Review. J. Nanotechnology, vol. 2013, no. 296517, 2013, pp. 1–6.
16. Collins, Philip G.: Defects and Disorder in Carbon Nanotubes. Oxford Handbook of Nanoscience and Technology: Frontiers and Advances, Y.Y. Fu, eds., Oxford University Press, Oxford, England, 2009.
17. Lau, C.H., et al.: The Effect of Functionalization on Structure and Electrical Conductivity of Multi-Walled Carbon Nanotubes. J. Nanopart. Res., vol. 10, 2008, pp. 77–88.
18. Picozzi, Silvia, et al.: Ozone Adsorption on Carbon Nanotubes: Ab Initio Calculations and Experiments. J. Vac. Sci. Technol. A., vol. 22, no. 4, 2004, pp. 1466–1470.
19. Arai, Susumu; Saito, Takashi; and Endo, Morinobu: Effects of Additives on Cu-MWCNT Composite Plating Films. J. Electrochem. Soc., vol. 157, no. 3, 2010, pp. D127–D134.
20. Cho, Youngmi, et al.: Electronic Structure Tailoring and Selective Adsorption Mechanism of Metal-Coated Nanotubes. Nano Lett., vol. 8, no. 1, 2008, pp. 81–86.
21. Neubauer, E., et al.: Potential and Challenges of Metal-Matrix-Composite Reinforced with Carbon Nanofibers and Carbon Nanotubes. Compos. Sci. Technol., vol. 70, no. 16, 2010, pp. 2228–2236.

22. Liu, Z.Y., et al.: Tensile Strength and Electrical Conductivity of Carbon Nanotube Reinforced Aluminum Matrix Composites Fabricated by Powder Metallurgy Combined With Friction Stir Processing. J. Mater. Sci. Technol., vol. 30, no. 7, 2014, pp. 649–655.
23. Chawla, S.; Naraghi, M.; and Davoudi, A.: Effect of Twist and Porosity on the Electrical Conductivity of Carbon Nanofiber Yarns. Nanotechnology, vol. 24, no. 25, 2013.
24. Chowdhury, Tamjid; and Rohan, J.F.: Influence of Carbon Nanotubes on the Electrodeposition of Copper Interconnects. ECS Trans., vol. 25, no. 38, 2010, pp. 37–46.
25. Timoshevskii, V., et al.: The Influence of Surface Roughness on Electrical Conductance of Thin Cu Films: An Ab Initio Study. J. Appl. Phys., vol. 103, no. 113705, 2008.
26. Shuai, Jing, et al.: Enhanced Strength and Excellent Transport Properties of a Superaligned Carbon Nanotubes Reinforced Copper Matrix Laminar Composite. Compos. Part A Appl. Sci. Manuf., vol. 88, 2016, pp. 148–155.
27. Aliev, Ali E., et al.: Thermal Conductivity of Multi-Walled Carbon Nanotube Sheets: Radiation Losses and Quenching of Phonon Modes. Nanotechnology, vol. 21, no. 3, 2010.
28. Subramaniam, Chandramouli, et al.: One Hundred-Fold Increase in Current Carrying Capacity in a Carbon Nanotube-Copper Composite. Nat. Commun., vol. 4, no. 2202, 2013.
29. Almansour, Amjad: Use of Single Tow Ceramic Matrix Minicomposites to Determine Fundamental Room and Elevated Temperature Properties. Ph.D. Thesis, Univ. of Akron, 2017.
30. Godin, Natalie; Reynaud, Pascal; and Fantozzi, Gilbert: Challenges and Limitations in the Identification of Acoustic Emission Signature of Damage Mechanisms in Composites Materials. Appl. Sci., vol. 8, no. 1267, 2018.
31. Maillet, Emmanuel, et al.: Feasibility and Limitations of Damage Identification in Composite Materials Using Acoustic Emission. Compos. Part A Appl. Sci. Manuf., vol. 75, 2015, pp. 77–83.
32. Gorven, Alastair; Almansour, Amjad; and Kiser, James: Using Acoustic Emission Energy and Frequency Analysis to Characterize Damage in SiC/SiC Minicomposites. Presented at the 43rd International Conference on Advanced Ceramics and Composites (ICACC), Daytona Beach, FL, 2019.
33. Miao, Menghe: Electrical Conductivity of Pure Carbon Nanotube Yarns. Carbon, vol. 49, no. 12, 2011, pp. 3755–3761.
34. Norasethasopon, S.; and Yoshida, K.: Finite-Element Simulation of Inclusion Size Effects on Copper Shaped-Wire Drawing. Mater. Sci. Eng. A, vol. 422, nos. 1–2, 2006, pp. 252–258.
35. Cao, Jien; Wang, Qian; and Dai, Hongjie: Electromechanical Properties of Metallic, Quasimetallic, and Semiconducting Carbon Nanotubes Under Stretching. Phys. Rev. Lett., vol. 90, no. 15, 2003.
36. Cullinan, Michael A.; and Culpepper, Martin L.: Carbon Nanotubes as Piezoresistive Microelectromechanical Sensors: Theory and Experiment. Phys. Rev. B, vol. 82, 2010, p. 115428.
37. Il'ina, M.V., et al.: Piezoelectric Response of Multi-Walled Carbon Nanotubes. Materials, vol. 11, no. 4, 2018, pp. 76–80.
38. Contes-de-Jesús, Enid, et al.: Platinum Electrodeposition on Unsupported Single Wall Carbon Nanotubes and Its Application as Methane Sensing Material. J. Electrochem. Soc., vol. 160, no. 2, 2012.
39. Park, Tae-Jin, et al.: Purification Strategies and Purity Visualization Techniques for Single-Techniques for Single-Walled Carbon Nanotubes. J. Mater. Chem., vol. 16, 2006, pp. 141–154.
40. Abel, Phillip B.: Ohmic Heating of Composite Candidate Graphite-Fiber/Coating Combinations. NASA TM–4491, 1993. https://ntrs.nasa.gov
41. Abel, Phillip B., et al.: Study of Copper on Graphite With Titanium or Chromium Bond Layer. J. Mater. Res., vol. 9, no. 3, 1994, pp. 617–624.
42. Wang, Jinlan, et al.: Transition-Metal-Catalyzed Unzipping of Single-Walled Carbon Nanotubes Into Narrow Graphene Nanoribbons at Low Temperature. Angew. Chem., vol. 50, no. 35, 2011, pp. 8041–8045.